Regulation of replicative histone RNA metabolism by the histone chaperone ASF1

Shweta Mendiratta, Dominique Ray-Gallet, Sébastien Lemaire, Alberto Gatto, Audrey Forest, Maciej Kerlin, Geneviève Almouzni

Regulation of replicative histone RNA metabolism by the histone chaperone ASF1

Shweta Mendiratta[1,4*], Dominique Ray-Gallet[1*], Sébastien Lemaire[1**], Alberto Gatto[1,5**], Audrey Forest[1], Maciej A. Kerlin[2,3,6] and Geneviève Almouzni[1,7***]

[1]Institut Curie, PSL Research University, Sorbonne Université, CNRS UMR3664, Laboratoire Dynamique du Noyau, Equipe Labellisée Ligue contre le Cancer, 75005 Paris, France

[2]Institut Curie, PSL Research University, Sorbonne Université, CNRS UMR3664, Laboratoire Dynamique du Noyau, 75005 Paris, France.

[3]Institut Curie, PSL Research University, Sorbonne Université, CNRS UMR168, Laboratoire Physico Chimie Curie, 75005 Paris, France

[4]Present address: Department of Biochemistry and Molecular Medicine, Keck School of Medicine of the University of Southern California, Los Angeles, CA 90033, USA

[5]Present address: Roche Diagnostics, 2881 Scott Blvd, Santa Clara, CA 95050, USA

[6]Present address: Center for Integrative Genomics, University of Lausanne, Lausanne, Switzerland

[7]Lead Contact

*These authors contributed equally

**These authors contributed equally

***Corresponding author: genevieve.almouzni@curie.fr

SUMMARY

In S phase, duplicating and assembling the whole genome into chromatin requires upregulation of replicative histone gene expression. Here, we explored how histone chaperones control histone production in human cells to ensure a proper link with chromatin assembly. Depletion of the ASF1 chaperone specifically decreases the pool of replicative histones both at the protein and RNA levels. The decrease in their overall expression, revealed by total RNA-seq, contrasted with the increase in nascent/newly synthesized RNAs observed by 4sU-labeled RNA-seq. Further inspection of replicative histone RNAs showed a 3'-end processing defect with an increase of pre-mRNAs/unprocessed transcripts likely targeted to degradation. Collectively these data argue for a production defect of replicative histone RNAs in ASF1-depleted cells. We discuss how this regulation of replicative histone RNA metabolism by ASF1 as a "chaperone checkpoint" fine-tunes the histone dosage to avoid unbalanced situations deleterious for cell survival.

KEYWORDS: replicative histone, histone chaperone, Anti-Silencing Function 1 (ASF1), Chromatin Assembly Factor-1 (CAF-1), RNA metabolism, 3'-end processing.

INTRODUCTION

Histones are the protein components of the basic unit of chromatin, the core particle of the nucleosome, which consists of a $(H3\text{-}H4)_2$ tetramer flanked by two H2A-H2B dimers around which 147 bp of DNA wraps. [1,2] They play a central role in defining chromatin states associated with distinct cell fates. They are classified into replicative and non-replicative/replacement histone variants. While the latter do not exhibit S phase regulation in their expression, the replicative histone variants show a major peak in expression in early S phase to support chromatin assembly during genome replication. [3–5] Beside distinct regulation in expression timing, replicative and non-replicative histone genes also differ in their genomic organization and RNA structure. In most metazoans, the replicative histone genes organized in clusters lack introns [4–6] and are expressed in specialized nuclear bodies known as histone locus bodies (HLBs). [7,8] Their mRNAs do not contain a polyA tail but present a 3'conserved stem loop (SL) structure bound by Stem-Loop Binding Protein (SLBP), a key factor in replicative histone RNA metabolism. [4,6] These distinct features enable to provide the increase for histone supply ensuring nucleosome assembly during genome duplication in S phase. During the G1/S phase transition, a ~40-fold increment in histone mRNA levels involves the upregulation of both transcription and 3'-end processing. [9] This cell-cycle regulation also implicates Nuclear protein ataxia-telangectasia (NPAT) and Flice-associated huge protein (FLASH), the core components of the HLB. [4–6]

From their synthesis in the cytoplasm to their delivery to the chromatin or after eviction, histones are always escorted by histone chaperones. [10,11] This prevents free positively charged histones to engage into promiscuous interactions with acidic partners, notably with DNA, that

could form aberrant aggregates in the cell. During replication in human cells, two main chaperones ensure the deposition of H3-H4 onto DNA: Chromatin assembly factor 1 (CAF-1) comprising three subunits (p150/CHAF1A, p60/CHAF1B and p48) [12,13] and Anti-silencing factor 1 (ASF1), with two paralogs in mammals ASF1a and ASF1b [14] and originally identified in yeast. [15] Interestingly, on the one hand, ASF1 binds the newly synthesized replicative histones H3.1/H3.2-H4 to transfer them to CAF-1, for deposition in a DNA synthesis-coupled (DSC) manner. [16,17,18] On the other hand, ASF1 binds newly synthesized non-replicative histone H3.3 to transfer them to the Histone regulator A (HIRA) complex for deposition in a DNA synthesis-independent (DSI) manner. [16,19,20] In addition, ASF1 also promote histone recycling during replication and transcription. [21–23] Finally, in human cells, ASF1 but not CAF-1, also provides a buffering system for histone excess generated in response to stalled replication. [24] However, how these chaperones may impact histone RNA metabolism in mammals and other metazoans had remained unexplored. This is particularly interesting given that in budding yeast, where there are no distinct replicative and non-replicative H3 variants, the single ASF1 ortholog participates in activating histone gene transcription in S phase and transcriptional repression outside S phase in combination with Hir1, the budding yeast counterpart of HIRA. [25]

Here, by exploring in human cells the effect of depleting either ASF1 or CAF-1 on the protein and RNA levels of replicative histones, we find that ASF1 impacts the regulation of replicative histone RNA metabolism.

RESULTS

ASF1 depletion, in contrast to CAF-1 depletion, reduces replicative histones at the levels of both soluble protein and total RNA

We considered how, in mammals, particular features control replicative histone synthesis and usage from gene to chromatin (Figure 1A, scheme) and focused on ASF1 and CAF-1. We analyzed the effect of their respective depletion on replicative histones both at protein and RNA levels. For comparison, we also used conditions known to affect either the synthesis of replicative histones by depleting FLASH [26,27] or DNA replication by treating the cells with hydroxyurea (HU). [28] We transfected HeLa cells with siRNAs targeting ASF1a and ASF1b together (siASF1), the p60 subunit of CAF-1 (sip60), FLASH (siFLASH) or control (siCtrl). We depleted both ASF1a and ASF1b paralogs, since they most often compensate the depletion of the other. [14,29] We then performed a pulse of EdU, 48 hrs post-transfection with siRNA, or 24 hrs post-treatment with HU (0.1 mM) and harvested cells to analyze their cell cycle by FACS and their DNA replication by EdU labeling. We prepared proteins in either whole, cytosolic, nuclear and chromatin fractions, and in parallel total RNAs (experimental scheme Figure 1B). Whole cell extracts served to verify depletion efficiencies for ASF1 and CAF-1 p60 (Figure S1A). For FLASH, since the commercial antibodies we tested did not function in Western blot, we controlled the depletion efficiency by immunofluorescence. The presence of FLASH at HLBs [30], observed as foci in control cells, disappeared after siFLASH treatment (Figure S1A). FACS analysis showed an accumulation of cells in S phase in all conditions as compared to control cells (siCtrl and -HU), somewhat less pronounced for CAF-1 p60 depletion (Figure 1C). The defect in

S phase progression in all conditions correlated with the decrease of EdU labeling intensity as compared to controls, indicating replication alteration (Figures S1B and S1C).

We then estimated the amounts of the replicative histone H3.1 and H3.2 (recognized simultaneously by the same antibody) and of the non-replicative histone H3.3 in chromatin fraction and soluble cytosolic extract by Western blot. In chromatin fraction, all depletions reduced H3.1/H3.2, with ASF1 depletion giving the most extreme reduction (Figure 1D, left). Strikingly, in soluble cytosolic extract only ASF1 and FLASH depletions led to a strong decrease of H3.1/H3.2 (Figure 1D, right) without major changes for H3.3, except for FLASH depletion where H3.3 increased to possibly compensate the decrease of H3.1/H3.2 (Figure 1D). Thus, ASF1 depletion impacts replicative H3.1/H3.2 differently from HU-defect and from CAF-1 depletion. After HU treatment where DNA replication is altered, only a weak decrease of H3.1/H3.2 occurred in cytosolic extract while for CAF-1 p60 depletion, we rather saw an increase (Figure 1D, right). Indeed, under CAF-1 limitation, soluble H3.1/H3.2 likely accumulate due to defect in deposition. The decrease of cytosolic H3.1/H3.2, for FLASH and ASF1 depletions, prompted us to examine a role of ASF1 in replicative histone synthesis. We confirmed our findings by using different siRNAs targeting ASF1a and b (Figure S1D) and in soluble nuclear extracts (Figure S1E). Furthermore, given that cytosolic replicative histone H2B and H4 also decreased in ASF1-depleted cells (Figure S1F), ASF1 depletion may affect broadly most replicative histones in a coordinated fashion.

To examine effects at an RNA level, we performed RT-qPCR using total RNA to evaluate changes in the amount of replicative histone transcripts after ASF1, p60 and FLASH depletions or HU treatment. Total RNA corresponding to the replicative histone genes H2AC20, H1-4, H4C12 and H3C14 (encoding H2A, H1, H4 and H3, respectively) all decreased most

significantly in ASF1-depleted cells and in HU-treated cells (with the strongest decrease for siASF1) (Figure 1E). In contrast, total RNA did not decrease for the non-replicative histone genes H3-3A and H3-3B (both encoding H3.3) (Figure 1E). Moreover, we rescued the defect in replicative histones by expressing Strep-tagged ASF1a and b in siASF1-depleted HeLa cells (Figure S2A). Depleting SLBP, also involved in regulating replicative histone synthesis [31,32], compared to FLASH depletion in FACS, EdU labeling and replicative histones at both protein and RNA levels (Figures S1A and S2B-S2F). Depleting independently either ASF1a or ASF1b, did not match the double depletion (Figures S1A and S2B-S2F). Since both ASF1 and HIRA in yeast regulate transcription of histone genes [25] and HIRA in mammals is a negative regulator of replicative histones [33], we also depleted HIRA. However, HIRA depletion did not alter FACS or EdU labeling and did not impact replicative histones at both protein and RNA levels (Figures S1A and S2B-S2F).

We conclude that ASF1 depletion, but not CAF-1 depletion nor HU treatment, modulates the levels of both total RNA and soluble protein corresponding to replicative histone genes. Thus, the impact of ASF1 depletion on replicative histones cannot be reproduced by a chromatin assembly defect or a replication stress.

ASF1 depletion reduces the expression of most annotated replicative histone genes at a transcriptome level during S phase

We compared RNA-seqs from siCtrl- and siASF1-transfected asynchronous cells including spike in controls (Figure 2A). Differential gene expression analysis revealed global transcriptional changes after ASF1 depletion (Figures 2A, S3A and S3B). Pathways associated with cell cycle progression, most notably MYC-driven pathways, ranked among the top downregulated. Instead,

among the top upregulated pathways, tumor necrosis factor alpha (TNFα) signaling and the p53 pathway proved enriched, in line with their roles in cell cycle arrest. Interestingly, the non-replicative histone gene H1-0, normally reduced in cells with long-term self-renewal ability and tumorigenic potential [34,35], was also upregulated. Altogether, these changes are consistent with the reduced proliferation and slow S phase completion observed in ASF1-depleted cells. [22,24] The noticeable reduction in the expression level of replicative histone genes after ASF1 depletion caught our attention, with replicative histones enriched among the top significantly downregulated genes (Figure 2A and Table S1). To better characterize the effect of ASF1 depletion on gene expression along S phase, we then generated total RNA-seq data from cells synchronized at G1/S arrest (0 hr) by double thymidine block and released until early (2 hrs) and mid S phase (5 hrs) (scheme and FACS Figure 2B). Of note, around half the number of cells in siASF1 condition enter S phase after release as compared to siCtrl condition. For each time point we included spike in controls. Hierarchical clustering of differentially expressed genes after ASF1 depletion at different S phase stages identified six main groups (annotated 1 to 6) (Figures 2C, 2E and S3C): downregulated genes in groups 1, 2 and 3, and upregulated genes in groups 4, 5 and 6 (Table S1). Groups 1 and 2 comprised the top downregulated genes after ASF1 depletion with the strongest changes with S phase progression under control conditions (Figure 2E). Group 1 showed enrichment in genes involved in DNA replication. Group 2 stood out: it exclusively comprised 37 of the 59 replicative histone genes affected by ASF1 depletion among the 66 annotated replicative histone genes with detectable expression. This group 2 showed the largest differences in expression along S phase progression and under conditions of ASF1 depletion (Figures 2D and 2E). Indeed, under control conditions, replicative histone genes displayed their lowest expression levels in G1/S cells and the strongest induction after release

into S phase, progressively peaking from early (2 hrs) to mid S phase (5 hrs). ASF1 depletion led to a striking failure to increase the expression of all these genes after release. Additionally, we compared expression of all replicative histone genes with each other and with non-replicative histone genes (Figures S3D and S3E). We noted that, after ASF1 depletion, ten replicative histone genes, not clustered in Group 2, are also downregulated, and only five are unaffected.

Thus, ASF1 depletion has a strong effect on S phase-dependent genes, among which a large set of the annotated replicative histone genes.

ASF1 depletion increases replicative histones at the level of nascent/newly synthesized RNA

To consider the multiple levels in regulating replicative histone genes [5,6], we first explored ASF1 role at the level of transcription. While NPAT is crucial in regulating the transcription of replicative histone genes [36,37], FLASH has been involved in NPAT localization at HLBs [30]. By immunofluorescence, as expected, NPAT foci disappeared in FLASH-depleted cells while present in all the other conditions, and even brighter after ASF1 depletion as for FLASH foci (Figure S4). Thus, HLBs are maintained in ASF1-depleted cells. To analyze the newly transcribed RNAs, we performed 4-Thiouridine-labeled RNA-sequencing (4sU-labeled RNA-seq) in asynchronous cells 48 hrs after siRNA transfection including spike-in controls (experimental scheme Figure 3A). To our surprise, ASF1 depletion led to increased levels of nascent/newly synthesized RNAs for replicative histone genes (Figure 3A). This was surprising given the decrease in their expression observed by RNA-seq and RT-qPCR using total RNA. We compared heatmaps from this 4sU-labeled RNA-seq and the previous total RNA-seq (Figure 2A), using the hierarchical clustering with 6 groups as for the total RNA-seq using synchronized cells (Figure 2C). Strikingly, group 2 which comprises most replicative histone

genes exhibited an opposite behaviour in 4sU-labeled and total RNA-seqs (Figures 3B and 3C). While most replicative histone genes affected by ASF1 depletion showed this peculiar behaviour, this was not the case for non-replicative histone genes (Figure 3C). Comparing total and 4sU-labeled RNA-seqs (Figure 3D), most genes showed the same behaviour in both datasets, including non-replicative histone genes. In sharp contrast, while downregulated in total RNA-seq, the replicative histone genes stood out with a clear upregulation in 4sU-RNA-seq. Of note, in contrast to total RNAs, which steady state levels reflect transcription, processing and decay, the amount of nascent/newly synthesized RNAs depends on transcription but in the case of short genes such as replicative histone genes, also depends on processing. Thus, our data suggest that an increase in nascent/newly synthesized transcripts for the replicative histones after ASF1 depletion corresponds either to a higher transcription or to an accumulation of newly synthesized replicative histone transcripts, possibly because of a processing defect, or both.

In conclusion, while ASF1 depletion led to a decrease in total transcripts corresponding to replicative histones, our latter results showed that when considering nascent/newly synthesized RNAs, their amounts rather than reducing, they even increased. These data prompted us to explore whether ASF1 may impact the 3'-end processing of replicative histone pre-mRNAs.

ASF1 depletion affects the 3'-end processing of replicative histone pre-mRNAs

In metazoans, replicative histone transcripts are not polyadenylated and associated with a unique post-transcriptional regulation. [4] The 3'-end processing of replicative histone pre-mRNAs occurs with a cleavage between the stem loop (SL) and the histone downstream element (HDE) to produce mRNAs with the SL and deprived of the sequence downstream the cleavage site and

notably the HDE [4] (Figure 1A). We performed a metagene analysis for all replicative histones to be able to provide the average change in RNA reads when comparing siCtrl to siAsf1. This plot shows unambiguously a higher fold change in region 3' of the SL when compared to region within the replicative histone gene in both total and 4sU-labeled RNA-seqs (Figure 4A). This is illustrated in individual snapshots from genome browser corresponding to individual genes (Figure S5A). By measuring the fraction of fragments overlapping the cleavage site between the SL and the HDE, we could confirm the presence of a higher fraction of unprocessed pre-mRNAs in both asynchronous total and 4sU RNA-seqs as well as in total RNA-seq from synchronized cells (Figure S5B). Taken together these analyses are consistent with an increase of unprocessed transcripts when ASF1 is depleted.

Disruption of the 3'-end processing of replicative histone pre-mRNAs enables polyadenylation at a distal polyA site [38–41] or oligoadenylation when proceeding towards degradation by the RNA exosome. [42,43] Here, we found reads from replicative histone transcripts with long stretches of adenines. The number of these reads, hereafter designated as oligo/polyadenylated reads, increased after ASF1 depletion (Figure S5C, left) while the level of adenylated RNAs of other highly expressed genes did not change (Figure S5C, right). This finding further supports an impact of ASF1 depletion on the 3'-end processing of replicative histone RNAs.

To confirm the 3'-end processing defect, we performed RT-qPCR for two different replicative histone genes, H1-4 and H3C14, using primers allowing to amplify only pre-mRNAs/unprocessed transcripts (primers "pre" located downstream the cleavage site) (scheme Figure 4B). By using total RNAs from siRNA-transfected or HU-treated cells (scheme Figure 1B), we found that the amount of pre-mRNAs/unprocessed RNAs significantly increased

after siASF1 and siFLASH transfections as compared to siCtrl but not after siCAF-1 transfection or HU treatment (Figure 4B). This argues that ASF1 depletion affects the 3'-end processing of replicative histones, as previously demonstrated for FLASH depletion. [26,27] In agreement with the fact that the replicative histones remained unaffected after single depletions (siASF1a or siASF1b alone) or HIRA depletion, we did not detect any increase of unprocessed transcripts under these conditions while SLBP depletion led to some increase (Figure S5D).

Therefore, we conclude that ASF1 depletion affects the 3'-end processing of the replicative histone pre-mRNAs.

DISCUSSION

Here, we discovered a role for the histone chaperone ASF1 in regulating specifically the expression of replicative histone genes. As illustrated in Figure 4C, ASF1 depletion led to increased amount of nascent/newly synthesized replicative histone RNAs while the amount of total RNAs decreased, resulting subsequently in a decrease of replicative histone proteins. Moreover, ASF1 depletion affects the 3'-end processing of replicative histone pre-mRNAs. This is very distinct from CAF-1 depletion which acts solely at the deposition level downstream of ASF1 (Figure 4C). Our data thus argue for a specific role of ASF1 in mammals in controlling the expression of replicative histone genes by regulating their RNA metabolism.

The increase of nascent/newly synthesized replicative histone transcripts in ASF1-depleted cells can be due to the accumulation of unprocessed transcripts (still not degraded) or to an increase in transcription of the corresponding genes, or both. We found that the decrease of total replicative histone transcripts reflects a defect of their 3'-end processing and their targeting to degradation, at least in part, via the RNA exosome (preliminary data). The exact cause of this defect remains unknown, and we do not exclude a possible consequence of a transcriptional defect. However, a direct role of ASF1 in the 3'-end processing of replicative histone RNAs is supported by the identification of ASF1 in a screen for factors involved in replicative histone pre-mRNA processing in Drosophila.[44] The fact that depleting key processing factors specific of replicative histone pre-mRNAs like FLASH and SLBP leads to phenotypes that compared to ASF1 depletion further connects ASF1 to the replicative histone RNA processing. Indeed, FLASH or SLBP depletions, both lead to a decrease in replicative histones, slower S phase progression and ssDNA formation defects in response to replication inhibitors as observed in

cells lacking ASF1.[45] However, ASF1 depletion reduces more severely levels of total RNAs corresponding to replicative histone genes as shown by RT-qPCR (Figure 1E), indicating a higher degradation of the replicative histone RNAs when compared to FLASH- and SLBP-depleted cells. In contrast, the differences between a HU treatment, that affects DNA replication, and siASF1 transfection argue that the impact of ASF1 depletion on replicative histone RNA metabolism is not just a mere consequence of DNA replication slowing down. Future work should dissect further how and where ASF1 intervenes in the RNA metabolism specific of the replicative histone genes.

Previous reports showed that both ASF1 and CAF-1 depletions affect S phase progression due to nucleosome assembly defects during replication.[22,24,46] We should now integrate that ASF1 depletion impacts expression of replicative histone genes which could by itself also contributes to the defect of S phase progression. Of note, arrest in S phase progression upon overexpression of the histone chaperone HIRA had been linked to defect in the expression of replicative histone genes.[33] While at first, these observations had led to propose that HIRA acted as a repressor of replicative histone gene expression, as reported in yeast[47,48], alternative explanations could build on our results. Indeed, overexpression of the HIRA mutant unable to interact with ASF1[20] cannot interfere with the expression of replicative histone genes.[33] Thus, considering our new findings, the difference between overexpression of HIRA wild type and HIRA lacking ASF1 interaction, could reflect the trapping of ASF1 by HIRA, preventing ASF1 to stimulate the replicative histone gene expression. Notably, we did not detect any effect of HIRA depletion on replicative histones arguing against its direct role as a repressor of their expression in human cells. Finally, the histone chaperone nuclear autoantigenic sperm protein (NASP), found together with ASF1 in a multichaperone complex[24], protects soluble H3-H4

proteins against degradation but its depletion does not affect the cell cycle [49], which is clearly different from ASF1 depletion. More generally, the role of ASF1 in the synthesis of replicative histones offers a different framework for the interpretation of previous observations linked to ASF1 defects. Indeed, most transcriptomic data have been generated from poly(A+) RNAs and usually do not include replicative histone RNAs, and thus several studies probably missed the impact of ASF1 on the expression of replicative histone genes. Notably, the upregulation of ASF1a or ASF1b observed in various cancers [14,50] that gives tumoral cells a proliferation advantage, may actually relate to a combined stimulation of both replicative histone synthesis and deposition processes, an aspect under-explored in tumorigenesis. We postulate that fine tuning ASF1 dose and function would thus provide the cell with an ingenious way to prevent imbalance in histone provision. Coupling replicative histone expression to ASF1 availability would represent a "chaperone checkpoint" to control the histone flow during S phase thereby preventing excess of free replicative histones that could be deleterious for the cell.

LIMITATIONS OF THE STUDY

We find a role for ASF1 in the RNA metabolism of replicative histone genes during S phase. However, how cell cycle influences this role, and the exact molecular mechanism remains to be deciphered, including a link between ASF1 and specific components of the 3'-end processing of replicative histone RNAs. Our study also shows that the effect of ASF1 applies broadly to all type of replicative histones from the histone clusters. To examine individually genes in each cluster, it will be interesting to quantify replicative histone RNAs using single molecule RNA FISH and to determine whether a similar role in RNA metabolism could be assigned to other histone chaperones and in particular H2A-H2B chaperones. Finally, following our analysis on

cultured cells it would be exciting to explore the function of ASF1 on replicative histone RNA metabolism in other cells, during development, in non-tumoral primary cells, in ESCs and especially in cancer cells with described overexpression of ASF1.

ACKNOWLEDGMENTS

We thank Antoine Coulon and Kyra Borgman for support on RNA analysis. This work was supported by the ERC-2015-ADG-694694 "ChromADICT", the Ligue Nationale contre le Cancer (Equipe labellisée Ligue), ANR-11-LABX-0044_DEEP and ANR-10-IDEX-0001-02 PSL. S.M. was supported by ANR-16-CE11-0028 "REPLICAF" and ERC-2015-ADG-694694 "ChromADICT", A.G. by H2020 Marie Skłodowska-Curie Actions grant agreement 798106 "REPLICHROM4D" and ERC-2015-ADG-694694 "ChromADICT".

AUTHOR CONTRIBUTIONS

Conceptualization, S.M., D.R.-G., G.A.; Investigation, S.M., D.R.-G., A.F. and M.A.K.; Software and Data Curation, A.G. and S.L.; Formal analysis, S.L.; Writing-Original draft, S.M., A.G., D.R.-G. and G.A.; Writing-Review & Editing, D.R.-G., S.L. and G.A.

DECLARATION OF INTERESTS

The authors declare no competing interests.

FIGURE LEGENDS

Figure 1. ASF1 depletion reduces replicative histones at the levels of both protein and total RNA

(A) Scheme for replicative histones genes, their transcription, protein synthesis and incorporation into chromatin. Intron less replicative histone genes in multiple copies are organized in clusters on chromosomes 6 (HIST1) and 1 (HIST2 and HIST3). Their pre-mRNAs are cleaved downstream of a conserved stem loop (SL) and upstream of a purine rich Histone Downstream Element (HDE). Their mRNAs lack polyadenylation in metazoans. After translation, ASF1 interacts with soluble replicative H3-H4 dimers and transfers them to CAF-1 to form nucleosomes on replicated DNA, in a DNA synthesis dependent pathway mainly at the replication fork during S phase. **(B)** Experimental strategy. We transfected human HeLa cells with siRNA or treated them with HU (0.1 mM). 48 hrs after siRNA transfection or 24 hrs after HU treatment, we added EdU for a 20 mins pulse. We performed FACS, EdU labeling, protein, and total RNA preparation. **(C)** FACS of cells 48 hrs after siRNA (siCtrl, siASF1, siCAF-1-p60 or siFLASH) or 24 hrs after HU (+HU) treatments or control (-HU). With PI-stained cells for DNA content and flow cytometry, we estimated G1, S and G2/M cells (%). **(D)** Western blot analysis of chromatin fraction and cytosolic extract from cells 48 hrs after siRNA (siCtrl, siASF1, siCAF-1-p60 or siFLASH) or 24 hrs after HU (+HU) treatments or control (-HU). We used 10 and 20 µg of extracts and γ-tubulin as loading control. We indicated the fold change average for H3.1/H3.2 and H3.3 (for cytosolic extracts and chromatin fraction) and H3.3:H3.1/H3.2 ratio (for chromatin fraction). **(E)** RT-qPCR analysis of histone RNA levels. We isolated total RNA from HeLa cells 48 hrs after siRNA (siCtrl, siASF1, siCAF-1-p60 or siFLASH) or 24 hrs after HU (+HU) treatments or control (-HU). We showed four replicative genes

(in black) H2AC20 (encodes H2A type 2-C), H1-4 (encodes H1.4), H4C12 (encodes H4) and H3C14 (encodes H3.2), and the two non-replicative genes (in white) H3-3A and H3-3B (both encode H3.3). The fold change in transcript relative to siCtrl or Control (-HU) corresponds to the mean of three independent biological replicates, error bars show standard deviation. We estimated the fold changes significance with a "two.sided" Student test. P-value legend is ***: <0.001, **: <0.01, *: <0.05, NS: >= 0.05. See also Figures S1 and S2.

Figure 2. ASF1 depletion reduces total RNA corresponding to replicative histone genes

(A) (Left top) Scheme for the RNA-seq analysis from asynchronous cells. Hela cells transfected with siRNA (siCtrl or siASF1) and harvested 48 hrs later to prepare total RNA for sequencing. **(Left bottom)** ASF1 depletion efficiency verified by Western blot analysis on whole cell extract from siCtrl- and siASF1-treated cells. We loaded extracts for the same numbers of cells (1x, 2x and 4x). **(Right)** Volcano plot illustrating the decrease in expression of replicative histone genes after ASF1 depletion from asynchronous cells. For all the genes expressed in at least 2 samples, we provided statistical significance (y-axis, -log10 of FDR) and difference in total RNA (x-axis, log2 fold change) between siASF1 and siCtrl conditions. We highlighted the top 10 significant replicative histone genes affected, ranked by statistical significance, and indicated the replicative histone genes H4C12 and H3C14 and the non-replicative histone genes H3-3A and H3-3B, analysed by RT-qPCR (Figure 1E). **(B) (Left)** Scheme for the RNA-seq analysis on synchronized cells. After siRNA (siCtrl or siASF1) on day 1, we synchronized cells with a double thymidine block and harvested them on day 3 at 0 (G1/S), 2 and 5 hrs (S phase) after the second thymidine block release, to prepare and sequence total RNA. **(Right)** FACS of cell synchronized in the different conditions. **(C)** Heat map of gene expression in siCtrl and siASF1 at different time points

after synchronization and release into S phase for differentially expressed genes (columns) ordered by hierarchical clustering, including all genes showing significant differences at FDR < 0.05. The color gradient is proportional to each gene expression in each sample, relative to their average across all samples (log2 normalized counts, mean-centred and reduced): from blue (lower than average) to red (higher than average). We indicated the six groups of genes, identified based on hierarchical clustering (top six column clusters). We used replicate 1 (R1) and replicate 2 (R2) experiments. **(D)** Zoom on the heat map from panel (C), focus on group 2 with only replicative histone genes. Color gradient shows relative expression as in (C). **(E)** Expression along S phase in siCtrl (blue) and siASF1 (red) conditions for the six groups defined in panel (C). In each graph, we showed the distribution of the genes in each group based on their relative expression averaged on the two replicates and centred on 0. S phase time are 0 (G1/S), 2 and 5 hrs (S phase) after release from G1/S. Values as in panels (C) and (D). See Figure S3C for Gene ontology (GO) for each group. See also Figure S3 and Table S1.

Figure 3. ASF1 depletion increases nascent/newly synthesized RNA for replicative histones

(A) (Left) Scheme for 4sU-labeled RNA sequencing [51] 48 hrs after siRNA transfection (siCtrl or siASF1). **(Right)** Relative nascent/newly synthesized RNA level (mean-centred counts, normalized and log2 transformed) of replicative histone genes from 4sU-labeled RNA-seq performed in control condition (siCtrl) and after ASF1 depletion (siASF1). For each replicate (R1 and R2), the box plot shows the distribution of replicative histone genes. **(B)** Heat maps of RNA level from 4sU-labeled RNA-seq (top) and from total RNA-seq (Figure 2A) (bottom). Genes set ordered in six groups as in Figure 2C for differentially expressed genes using total RNA-seq from synchronized cells. Colour gradient shows expression relative to average at the same scale than in Figure 2C (log2 normalized

counts, mean-centred and reduced): from blue (lower than average) to red (higher than average). We showed duplicate (R1 and R2). **(C)** Zoom on heat maps from panel (B) focusing on Group 2 and heat maps for non-replicative histone genes for comparison. Nascent/newly synthesized RNAs assessed by 4sU-labeled RNA-seq (pulse), for the short replicative histone genes, depend on transcription and processing. Total RNAs assessed by total RNA-seq (steady-state) depend on transcription, processing, and decay. **(D)** Scatter plot for genes according to their fold changes in total RNA and in 4sU-labeled RNA in asynchronous cells with Group 2 replicative histones in purple and non-replicative histones highlighted in green. Genes on the red line have equal fold changes in both total and 4sU-labeled RNA-seqs. See also Figure S4.

Figure 4. ASF1 depletion affects the 3'-end processing of replicative histone transcripts

(A) Metagene analysis of replicative histone genes of Group 2 in total and 4sU-labeled RNA-seqs. We provided fold change in siASF1 relatively to siCtrl in the replicative histone gene (TSS to SL) and in the region downstream of the SL. Solid and dashed lines correspond to replicates R1 and R2, respectively. **(B) (Top)** Scheme for replicative histone pre-mRNA and its 3'-end processing, with cleavage downstream of the Stem-Loop (SL) and upstream of the Histone Downstream Element (HDE). For the RT-qPCR, "pre" primers before the SL and downstream of the cleavage site amplify pre-mRNAs/unprocessed transcripts. **(Bottom)** RT-qPCR for replicative histone pre-mRNAs/unprocessed transcripts with "pre" primers on genes H1-4 and H3C14. We used total RNA from HeLa cells 48 hrs after siRNA (siCtrl, siASF1, siCAF-1-p60 or siFLASH) or 24 hrs after HU (+HU) treatments or control (-HU) (Figure 1B). Fold changes in unprocessed transcript for siASF1, sip60 and siFLASH transfected cells relatively to siCtrl, or for cells treated with HU (+HU) relatively to non-treated cells (-HU) correspond to means for three independent biological replicate

experiments, error bars show standard deviation. Student test provides the significance for siASF1 having a higher fold change than in another condition. P-value legend is ***: < 0.001, **: < 0.01, *: < 0.05, NS: >= 0.05. **(C)** Model to summarize the impact of CAF-1 and ASF1 depletions on the synthesis and usage of replicative histones during S phase. ASF1 depletion leads to an accumulation of newly synthesized pre-mRNAs/unprocessed transcripts, likely targeted to degradation, and a lack of mature mRNAs due to a 3'-end processing defect (1), leading to reduced levels of soluble replicative histones (2) and ultimately a decrease of nucleosomal replicative histones due to the decrease of both synthesis and usage (histone deposition) of replicative histones (3). In contrast, CAF-1 depletion does not affect the replicative histone RNA metabolism (1) but leads to an accumulation of soluble replicative histones (2) most likely due to a defect of usage (histone deposition) reflected by a decrease of nucleosomal replicative histones (3). See also Figure S5 and Table S1.

STAR METHODS

KEY RESOURCES TABLE

REAGENT or RESOURCE	SOURCE	IDENTIFIER
Antibodies		
ASF1a	Cell Signaling	Cat#2990
ASF1b	Agrobio	Groth et al [24]
H3.1/2	Active Motif	Cat#61629
H3.3	Millipore	Cat#09-838
H4	Abcam	Cat#ab31830
H2B	Abcam	Cat#ab1790
p60 (CAF-1)	Agrobio	Groth et al [24]
FLASH	Sigma	Cat#HPA053573
SLBP	Abcam	Cat#ab181972
HIRA	Active Motif	Cat#WC119.2H11
NPAT	Invitrogen	Cat#PA5-66839
γ-tubulin	Sigma	Cat#T5326
Vinculin	Sigma	Cat#V9131
Chemicals, peptides, and recombinant proteins		
Hydroxyurea (HU)	Sigma	Cat#H 8627
Lipofectamine RNAiMAX	Invitrogen	Cat#13778-150
Lipofectamine 2000	Invitrogen	Cat#11668-019
4-Thiouridine (4sU)	Sigma	Cat#T4509
Dulbecco's Modified Eagle's Medium (DMEM)	Gibco	Cat#41966
Opti-MEM, Reduced Serum Medium	Gibco	Cat#31985
Vectashield, Antifade Mounting Medium	Vector Laboratories	Cat#H-1000
Protein Assay Dye Reagent Concentrate	Bio-Rad	Cat#5000006
SuperSignal™ West Pico PLUS Chemiluminescent Substrate	Thermo Fisher Scientific	Cat#34580
FxCycle™ PI/RNase solution	Invitrogen	Cat#F10797
RNase-free DNase	QIAGEN	Cat#79254
TURBO DNA-free kit	Thermo Fisher Scientific	Cat#AM1907
Protease Inhibitor Cocktail Tablets - Complete, EDTA-free	Roche-Merck	Cat#05056489001
Phosphatase Inhibitor Cocktail Tablets - PhosSTOP EasyPack	Roche-Merck	Cat#04906837001
Pierce Reversible Stain	Thermo Fisher Scientific	Cat#1858784
Critical commercial assays		
Click-iT™ EdU Alexa Fluor™ 594 Imaging Kit	Invitrogen	Cat#C10339
RNeasy Plus Mini Kit	QIAGEN	Cat#74134
SuperScript™ III First Strand Synthesis SuperMix	Invitrogen	Cat#11752-050
PowerSYBR Green PCR Master Mix	ABI	Cat#4367659
Deposited data		
RNA-seq data	ArrayExpress	E-MTAB-12501
Raw data, Western blots and microscope images	Mendeley data	https://doi.org/10.17632/2bbvdfrrct.1

Experimental model: Cell line		
Human: HeLa	ATCC	CC-L2
Oligonucleotides		
ON-TARGETplus Non-targeting control siRNA UGGUUUACAUGUCGACUAA	Dharmacon	Cat#D-001810-01
ON-TARGETplus ASF1a siRNA #1 GUGAAGAAUACGAUCAAGUUU	Dharmacon	Groth et al [22]
ON-TARGETplus ASF1a siRNA #2 GAGACAGAAUUAAGGGAAAUU	Dharmacon	Groth et al [22]
ON-TARGETplus ASF1a siRNA #3 (3'UTR) CCUGAAAUUCCGUAAGUAUU	Dharmacon	This paper
ON-TARGETplus ASF1b siRNA #1 CAACGAGUACCUCAACCCUUU	Dharmacon	Groth et al [22]
ON-TARGETplus ASF1b siRNA #2 CGGACGACCUGGAGUGGAAUU	Dharmacon	Groth et al [22]
ON-TARGETplus ASF1b siRNA #3 (3'UTR) CCUUGAGUACCAUUGAUCUU	Dharmacon	This paper
ON-TARGETplus FLASH siRNA CCGCAAGGAUGAAGAAAUAUU	Dharmacon	Mejlvang et al [45]
ON-TARGETplus SLBP siRNA GGAUGUGAUUUGCAAGAAAUU	Dharmacon	Mejlvang et al [45]
ON-TARGETplus p60 CAF-1 siRNA GCGUGUGGCUUUCAAUGUUUU	Dharmacon	Polo et al [52]
ON-TARGETplus HIRA siRNA GGAUAACACUGUCGUCAUC	Dharmacon	Ray-Gallet et al [53]
Primer H2AC20 Forward GCTCGGGACAACAAGAAGAC	Sigma	This paper
Primer H2AC20 Reverse ATTTGCTTTTGGCTTTGTGG	Sigma	This paper
Primer H4C12 Forward TACTGCGCGACAATATCCAG	Sigma	This paper
Primer H4C12 Reverse CAACCACCGAAACCGTAGAG	Sigma	This paper
Primer H1-4 Forward TTCAACATGTCCGAGACTGC	Sigma	This paper
Primer H1-4 Reverse AGGCGGCAACAGCTTTAGTA	Sigma	This paper
Primer H1-4-pre Forward CTAAACCAAAGACCGCCAA	Sigma	This paper
Primer H1-4-pre Reverse ATAGTGCAACAGCTCTTTTACTG	Sigma	This paper
Primer H3C14 Forward GCTGGTAAGCCTGTGTTTTGG	Sigma	Ruepp et al [54]
Primer H3C14 Reverse GCCGCCGGTCGACTT	Sigma	Ruepp et al [54]
Primer H3C14-pre Forward TTCCATCGTATCCAAAAGGCTCTT	Sigma	Ruepp et al [54]
Primer H3C14pre Reverse CAAGCGGTACAGCTTCTTCC	Sigma	Ruepp et al [54]
Primer H3C1 Forward AGATCCGCCGTTATCAGAAGTC	Sigma	This paper
Primer H3C1 Reverse CAGGCGCTGGAAAGGTAGTT	Sigma	This paper

Primer H3-3A Forward TAAAGCACCCAGGAAGCAAC	Sigma	Cook et al [49]
Primer H3-3A Reverse AGGGAAGTTTGCGAATCAGA	Sigma	Cook et al [49]
Primer H3-3B Forward AAGCTGCCCTTCCAGAGGTT	Sigma	Cook et al [49]
Primer H3-3B Reverse ACCTCAGGTCGGTTTTGAAATC	Sigma	Cook et al [49]
Primer PPIA Forward CATCTGCACTGCCAAGACTGA	Sigma	Simeonova et al [55]
Primer PPIA Reverse TTCATGCCTTCTTTCACTTTGC	Sigma	Simeonova et al [55]
Primer RPLPO Forward CTTGTCTGTGGAGACGGATTACAC	Sigma	Simeonova et al [55]
Primer RPLPO Reverse TACGCCAAGAAGGCCTTGA	Sigma	Simeonova et al [55]
Recombinant DNA		
Plasmid: pEXPR-IBA105	IBA	N/A
Plasmid: pEXPR-IBA105-ASF1a	IBA	Groth et al [22]
Plasmid: pEXPR-IBA105-ASF1b	IBA	Groth et al [22]
Software and algorithms		
ImageJ (1.53)	ImageJ	http://imagej.nih.gov/ij
FlowJo (10.9.0)	BD Biosciences	http://www.flowjo.com/
Image Lab (6.1.0)	Bio-Rad Laboratories	N/A
Python (3.9.5)	Python Software Foundation	https://www.python.org/downloads/release/python-395/
R (4.2.1)	R Project	https://www.r-project.org/
Hisat2 (2.2.0)	Kim Lab @ UT Southwestern	http://daehwankimlab.github.io/hisat2/
Bedtools (2.30.0-13)	Quinlann Lab @ U. of Utah	https://github.com/arq5x/bedtools2/releases
Bowtie2 (2.4.4)	Johns Hopkins University	https://bowtie-bio.sourceforge.net/bowtie2/index.shtml
Samtools (1.12)	Sanger Institute	https://www.htslib.org/
FeatureCounts (2.0.2)	University of Melbourne	https://subread.sourceforge.net/featureCounts.html
Original code	N/A	https://doi.org/10.5281/zenodo.10412865
Other		
Dynabeads™ M-280 Streptavidin	Invitrogen	Cat#11206D
QIAfilter Plasmid Maxi kit	QIAGEN	Cat#12263

RESOURCE AVAILABILITY

Lead Contact

For further information and requests for resources and reagents contact the lead contact, Geneviève Almouzni (genevieve.almouzni@curie.fr).

Materials availability

All materials and reagents generated in this study are available upon request.

Data and Code Availability

- Sequencing data from RNA-seq in ArrayExpress (accession: E-MTAB-12501) Raw images for Western blots and microscope images at Mendeley Data (https://doi.org/10.17632/2bbvdfrrct.1).
- This paper report original code at Zenodo DOI: https://doi.org/10.5281/zenodo.10412865.
- Any additional information required to reanalyze the data reported in this paper is available from the lead contact upon request.

EXPERIMENTAL MODEL AND STUDY PARTICIPANT DETAILS

Cell line

We used the human cervical carcinoma cell line HeLa (ATCC, CC-L2). We cultured cells in DMEM complete medium (Dulbecco's Modified Eagle's Medium with D-Glucose, L-Glutamine and Pyruvate) supplemented with 10% fetal calf serum, 100 U/mL Penicillin and 100 mg/mL Streptomycin. The HeLa cell line tested negative for mycoplasma contamination.

METHOD DETAILS

Cell synchronization, HU treatment, EdU labeling, siRNA and plasmid transfections

We synchronized the cells in G1/S via double thymidine block: sequential exposure to 2 mM thymidine (16-18 hrs), 24 mM 2-Deoxycytidine (6 hrs) and 2 mM thymidine (18 hrs). For hydroxyurea (HU) treatment, we added HU at a final concentration of 0.1 mM to the cells 24 hrs before harvesting. For replication sites labeling, we added EdU at a final concentration of 10 mM to the cells 20 mins before harvesting. We visualized EdU using the Click-iT EdU Alexa Fluor 594 imaging kit (C10339, Invitrogen). We used the ImageJ software to quantify EdU fluorescence intensity in images acquired using a Zeiss Apotome widefield microscope (63x objective) (~300 nuclei for each condition). We transfected cells with siRNA at 100 nM concentration using Lipofectamine RNAiMAX (Invitrogen, 13778-150) as shown in Clément et al[21] and with plasmids using Lipofectamine 2000 (Invitrogen, 11668-019). We listed sequences for siRNA in the Key resources table. We used Plasmids pEXPR-IBA105-ASF1a and -ASF1b expressing Onestrep-ASF1a and Onestrep-ASF1b, described in Groth et al [22].

FACS and immunofluorescence

After trypsinization, we counted cells using Vi-Cell XR Cell Viability Analyzer (Beckman coulter). We harvested around one million cells per condition using trypsin, fixed the cells with 70% cold ethanol and stained them with propidium iodide using FxCycle™ PI/RNase solution (ThermoFisher Scientific, F10797), according to manufacturer's instructions. We acquired data using FACS Attune NxT machine (ThermoFisher Scientific) and assessed cell cycle profile with FlowJo software (10.9.0).
For immunofluorescence, after permeabilizing cells 5 mins with 0.2% Triton in PBS, we blocked with BSA (5% in PBS plus 0.1% Tween) before incubation with primary and secondary antibodies and DAPI staining. We mounted coverslips in Vectashield medium and used a Zeiss Apotome widefield microscope (63x objective).

4sU-labeled RNA-seq and total RNA-seq

For the 4sU-labeled RNA-seq, we cultured cells in 15 cm dish and added 10 ml of new medium containing 1 mM 4sU for 8 mins. [51] After 8 mins, we lysed the cells, and prepared total RNA directly from

the cell culture dishes using the RNeasy Mini Kit according to the manufacturer's instructions. The total RNA was DNase treated using the TURBO DNA-free kit (ThermoFisher Scientific, AM1907) or by RNase-free DNase (QIAGEN, 79254) using manufacturer's instructions. The quantity of isolated RNA was measured using the Nanodrop and we checked the quality by Tapestation. For 4sU-labeled RNA purification, we used 100-200 µg RNA for RNA biotinylation and carried out purification using Streptavidin-coupled Dynabeads (11206D, Invitrogen). We used 10 ng of total and 4sU-labeled RNAs for library preparation using SMARTer Stranded Total RNA-seq kit and performed paired-end sequencing by the next-generation sequencing platform at Institut Curie, providing pairs of 101 bp long reads.

RNA-seq analysis

We aligned reads on the human reference genome (GRCh38 assembly) based on EnsEMBL gene annotation (release 95) with hisat2 (version 2.1.0), run in paired-end mode with default parameters. We computed gene-level counts from primary alignments with MAPQ > 2 using featureCounts (Subread package version 1.6.3) in paired-end mode with the '-s 2' option for reverse-stranded libraries. We aligned reads on the sequences of the ERCC92 RNA spike in control from Life Technologies. Raw counts, human genome, and spike in control together, were normalized for differences in library size (counts per million), then these library-normalized counts for every human gene were normalized across samples by spike in control fraction. For normalization we used edgeR (version 3.28.0). We assessed the effect of ASF1 depletion in asynchronous cells by differential expression analyses with edgeR on genes with a quantifiable signal as evaluated by the function 'filterByExpr' of the same package with default parameters. In synchronized cells, in addition, we evaluated differential gene expression after release into S phase in control or in ASF1 depletion for each time point as indicated. Full details are provided in Table S1 (sheet 1), along with the counts normalized by spike in controls for both asynchronous (sheet 2) and synchronous cells (sheet 3). For hierarchical clustering analyses in synchronous cells, we included any DEG showing significant difference in expression in any comparison. Normalized counts were used for hierarchical clustering via Ward's variance minimization method and for comparing the expression of replicative histone genes from total or 4sU-labeled RNA-seq data generated in asynchronous cells. Functional enrichment analyses were carried out (Table S1, sheets 6 to 9). All RNA-seq analyses were carried out with custom Python scripts. Pandas (version 0.24.2), NumPy (version 1.16.2), SciPy (version 1.3.1) and fastcluster (version 1.1.26) libraries were used for data manipulation, statistical analysis, and hierarchical clustering. Matplotlib (version 2.2.4) and Seaborn (version 0.9.0) were used for plotting and visualization. R packages were imported into Python using the rpy2 module (version 2.8.4).

Analysis of unprocessed replicative histone transcripts from RNA-seq

We used RNA-seq data, total and 4sU-labeled, to determine the proportion of unprocessed replicative histone transcripts in siCtrl and siASF1 conditions. We located for every replicative histone gene the human SL sequence 'GGC(C/T)CTTTTCAG(A/G)GCC' from Marzluff et al. [4] Then, we defined a region of 49 nucleotides from 20 nucleotides upstream of the SL sequence to 13 nucleotides downstream to reach the HDE, thus encompassing the cleavage site (scheme Figure S5B). We considered each RNA-seq fragment overlapping this region as indicative of an unprocessed transcript. For each replicative histone gene, we compared the number of reads mapping to the uncleaved 3' region of the gene, normalized by the window length, to the number of reads mapping on the ORF of the same gene, also normalized by the ORF length. Only fragments from concordant paired-end alignments, of length until 500 nucleotides and without gap (i.e., 'N' in the CIGAR string) in either of the two mate pairs were considered. Fragment counts were normalized across samples using DESeq2 median of ratios method. [56] We computed the fraction of unprocessed transcripts by dividing the normalized fragment counts overlapping the uncleaved 3' region by the normalized count of fragments mapping on the ORF of the corresponding replicative histone gene. Then, we compared the relative amounts of unprocessed transcripts in siCtrl and siASF1 from the RNA-seq data in either asynchronous or synchronized cells. We considered replicative histone gene if the minimal raw count obtained over the corresponding ORF across the samples was equal or over 45 and if the gene had at least one unprocessed transcript in siCtrl condition.

Analysis of oligoadenylated transcripts

We used total and 4sU-labeled RNA-seq data to determine the fractions of replicative histone mRNAs oligoadenylated in siCtrl and siASF1 conditions. We first identified fragments or read pairs that carry oligoadenylation signature. As the sequencing was reversed stranded, we looked in name-sorted alignments for pairs with the second read mapping in sense on replicative histone genes and filtered these pairs by first read carrying at least 22 'T's from the 5' end, which prevent selecting first reads matching in reverse any 'A' stretches present downstream of a few of replicative histone genes. Note that the first read may not map on genome because of the adenylation signature. The low amount of read pairs detected led us to sum per sample the counts over all the replicative histone genes. In addition, we normalized these counts using the spike in controls. For highly expressed genes, we calculated the average ranking of all genes throughout the samples. We could thus define the second decile of most expressed genes across the RNA-seq samples of synchronized cells.

Reverse transcription- quantitative PCR (RT-qPCR)

To obtain cDNA, we performed reverse transcription PCR using 1 µg of RNA for each sample using the SuperScript™ III First Strand Synthesis SuperMix (Invitrogen, 11752-050) according to manufacturer's instructions. We performed quantitative PCR using PowerSYBR Green PCR Master Mix (ABI, 4367659) with three technical replicates in 384-well plates using the QuantStudio 5 Real-Time PCR machine. We calculated relative expression by ΔΔct method, where we substracted the Ct values for PPIA endogenous control from each gene of interest (Δct) and then for normalization, we subtracted the Δct of the control (siCtrl) condition for each gene of interest (ΔΔct). We calculated relative expression as the fold change and plotted using $2^{(\Delta\Delta ct)}$. We listed primers in the Key resources. For a given condition, we estimated significance of the fold changes with a Student test ("t.test" function in R). The fold changes were log transformed prior to a comparison with the same distribution of the values centred on 0; or with the distribution of another condition in case of comparing two conditions. The tests are "two.sided" or oriented according the experiment.

Protein extraction and Western blotting

We prepared cytosolic and nuclear extracts from HeLa cells according to Martini et al [57] but using 300 mM NaCl for nuclear extracts. Briefly, after lysing cells in hypotonic buffer using Dounce homogenizer and centrifugation, we collected the supernatant (cytosolic extract) and treated the pellet with lysis buffer containing 300 mM NaCl. After centrifugation, the supernatant (nuclear extract) was collected, and the pellet treated with benzonase and sonicated. After centrifugation the supernatant containing the chromatin fraction was collected. We quantified extracts using Protein Assay Dye Reagent Concentrate (Bio-Rad, 5000006). For whole cell extracts, cells were resuspended in NuPAGE 1X LDS sample buffer supplemented with Sample reducing agent (invitrogen), treated with benzonase and sonicated. The samples were loaded on Bis-Tris 4-12% gel (NuPage, Invitrogen)) with PageRuler protein ladder. We run gels at 120 V for ~1.5 hrs and then transferred them onto a 0.2 µm nitrocellulose membrane using BioRad Turbo Transblot. Membranes were stained using Pierce reversible protein stain to check the transfer efficiency, blocked in 5% milk prepared in PBST for one hour at room temperature, then incubated in primary antibodies (Key resources table) diluted in 3% BSA-PBST at 4°C overnight on a rocker. Of note, for H3.3 and H3.1/2 Western blots, we incubated the same membrane first with the mouse anti-H3.1/2 antibody, then with the rabbit anti-H3.3 antibody. Membranes were then washed with PBST and incubated in secondary antibodies conjugated with horseradish peroxidase (HRP) with 5% milk PBST for one hour at room temperature. Secondary antibodies were prepared in dilutions of either 1:20,000 (rabbit) or 1:10,000 (mouse). Membranes were then washed with PBST, then exposed with SuperSignal West Pico PLUS chemiluminescent reagent. Membranes were imaged using ChemiDoc Touch system and processed with ImageLab software (Bio-Rad). We performed quantitative analysis of Western blots using tubulin normalization and estimated fold changes from at least three different Western blots and two different experiments.

Antibodies

For Western blots we used the following antibodies: ASF1a (1:2000, 2990, Cell Signaling), ASF1b (1:500, Agrobio[24]), H3.1/2 (1:500 for soluble extract and 1:5000 for chromatin fraction, 61629, Active Motif), H3.3 (1:500 for soluble extract and 1:5000 for chromatin fraction, 09-838, Millipore), H4 (1:500, ab31830, Abcam), H2B (1:1000, ab1790, Abcam), p60 CAF-1 (1:1000, Agrobio[24]), SLBP (1:500, ab181972,

Abcam), HIRA (1:100, WC119.2H11, Active Motif), γ-tubulin (1:2000, T5326, Sigma) and vinculin (1:1000, V9131, Sigma). For Immunofluorescence, we used the following antibodies: FLASH (1:300, HPA053573, Sigma) and NPAT (1:100, PA5-66839, Invitrogen).

QUANTIFICATION AND STATISTICAL ANALYSIS

Results of statistical tests are displayed by at least a symbol code on the corresponding panel (*: <0.05, **: <0.01, ***:<0.001, 'ns': non-significant). The p-value may be indicated below, or in the Figure legend to illustrate arguments. For genome wide comparisons, the p-values are presented in the Table S1. The type of statistical test depends on the comparison performed which is detailed in the following subsections. All the statistical tests were performed in R, with base statistical functions ('t.test' for mean comparison, 'glm' for applying a GLM) or with R packages indicated for the corresponding cases.

RNA-seq analysis

Differential expression analyses were performed with edgeR (version 3.28.0) on genes having a quantifiable signal as evaluated by the function 'filterByExpr' of the same package with default parameters. We assessed the effect of ASF1 depletion in asynchronous cells by fitting a quasi-likelihood negative binomial generalized log-linear model (GLM) comparing siASF1 to control.
To evaluate the effect of ASF1 depletion in synchronized cells before (0 hr) and after release into S phase (2 hrs), we similarly fitted a GLM including both additive and synergistic terms to model the stand-alone effect of S phase progression (changes in expression at 2 and 5 hrs relative to 0 hr) and ASF1 depletion (siASF1 relative to control across all time points), as well as at the specific effect of ASF1 depletion at different time points after release into S phase (siASF1 relative to control at 2 and 5 hrs). Full details about the variable encoding and GLM formulation are provided in Table S1 (sheet 1). For each effect, we applied a quasi-likelihood F-test on the respective GLM coefficient to assess its significance, followed by multiple testing correction via the Benjamini-Hochberg method (Table S1, sheet 4 for asynchronous cells and sheet 5 for synchronous cells). A false discovery rate (FDR) cut-off of 0.05 was used to identify differentially expressed genes (DEGs).
Functional enrichment analyses were carried out using the WebGestaltR package (version 0.4.2). For asynchronous cells, we evaluated the enrichment in Hallmark signatures from MSigDB by over-representation analysis (ORA) for the top 100 upregulated and top 100 downregulated genes, ranked by FDR (Table S1, sheets 6 and 7). For synchronous cells, we checked enrichment in biological processes associated to specific DEG clusters using Gene Ontology (GO) annotations (Table S1, sheets 8 and 9).

Analysis of unprocessed replicative histone transcripts from RNA-seq

Differential fraction of uncleaved transcripts was evaluated with a GLM (with gaussian family of link function) which considers the 'replicate identity', the 'condition' and the 'synergy' between the two. The p-value is the significance of the 'condition' term testing if this term has a coefficient greater than 0.

Metagene analysis of RNA-seq signal of replicative histones and downstream of their SL

We computed the coverage along the genome directly from the mapped reads, using "bedtools genomecov" command with options "-bga" and "-split". We recovered the coverage signal along the region from the TSS to 500 bases downstream of the SL of the replicative histone genes and normalized it based on sequencing depth and spike-in controls followed by a reduction to the geometric mean of expression of the set of genes. We then summarized in 20 bins by averaging the signal along the region from the TSS to the SL. Downstream of the SL, the signal is summarized in bins of 10 bases. We then compute the fold change from control to ASF1 depleted condition, in respect of the replicate, in every bin.

Reverse transcription-quantitative PCR (RT-qPCR)

For a given condition, significance of the fold changes was evaluated with a Student test ("t.test" function in R). The fold changes were log transformed prior to a comparison with the same distribution of the values centred on 0; or with the distribution of another condition in case of comparing two conditions. The tests are "two.sided" or oriented according the experiment.

ADDITIONAL RESOURCES

None.

Table S1. Analysis of RNA-seq data, related to Figures 2, 4, S3 and S5

Sheet 1: provides the summary of the next excel sheets; **Sheet 2** TMM (Trimmed Mean of the M-values)-normalized counts from total RNA-seq in asynchronous cells, related to Figures 3A, 3B, 3C and S3A; **Sheet 3:** TMM-normalized counts from total RNA-seq in cells synchronized at G1/S, related to Figures 2C, 2D, 2E, S3D and S3E; **Sheet 4:** Differential gene expression analysis comparing siASF1 with siCtrl samples using data from total RNA-seq in asynchronous cells, related to Figures 2A, 3D and S3B; **Sheet 5:** Differential gene expression analysis comparing siASF1 with siCtrl samples using data from total RNA-seq in cells synchronized at G1/S, related to Figure 2C; **Sheet 6:** Over-Representation Analysis (ORA) in hallmark signatures for the top 100 upregulated genes from total RNA-seq in asynchronous cells, related to Figure S3B; **Sheet 7:** Id to Sheet 6 but for the top 100 downregulated genes, related to Figure S3B; **Sheet 8:** Hierarchical clustering of differentially expressed genes (DEGs) in synchronized cells, related to Figures 2C, 2D, 2E, 3B, 3C, S3C and S3D; **Sheet 9:** For genes identified by hierarchical clustering (DEG clusters) in synchronized cells, their Over-Representation Analysis (ORA) in defined biological processes (Gene ontology classification), related to Figure S3C; **Sheet 10:** Signals (read counts) corresponding to 4sU-labeled RNA-seq spanning over the region downstream of the Stem Loop compared to the signals spanning over the ORF of the replicative histone gene expressed as a ratio, related to Figures 4A and S5A.

REFERENCES

1. Luger, K. (1997). Crystal structure of the nucleosome core particle at 2.8 A˚ resolution. *389*.

2. Zhou, K., Gaullier, G., and Luger, K. (2019). Nucleosome structure and dynamics are coming of age. Nat Struct Mol Biol *26*, 3–13. 10.1038/s41594-018-0166-x.

3. Armstrong, C., and Spencer, S.L. (2021). Replication-dependent histone biosynthesis is coupled to cell-cycle commitment. Proc. Natl. Acad. Sci. U.S.A. *118*, e2100178118. 10.1073/pnas.2100178118.

4. Marzluff, W.F., Wagner, E.J., and Duronio, R.J. (2008). Metabolism and regulation of canonical histone mRNAs: life without a poly(A) tail. Nat Rev Genet *9*, 843–854. 10.1038/nrg2438.

5. Mendiratta, S., Gatto, A., and Almouzni, G. (2019). Histone supply: Multitiered regulation ensures chromatin dynamics throughout the cell cycle. Journal of Cell Biology *218*, 39–54. 10.1083/jcb.201807179.

6. Marzluff, W.F., and Koreski, K.P. (2017). Birth and Death of Histone mRNAs. Trends in Genetics *33*, 745–759. 10.1016/j.tig.2017.07.014.

7. Hur, W., Kemp, J.P., Tarzia, M., Deneke, V.E., Marzluff, W.F., Duronio, R.J., and Di Talia, S. (2020). CDK-Regulated Phase Separation Seeded by Histone Genes Ensures Precise Growth and Function of Histone Locus Bodies. Developmental Cell *54*, 379-394.e6. 10.1016/j.devcel.2020.06.003.

8. Nizami, Z., Deryusheva, S., and Gall, J.G. (2010). The Cajal Body and Histone Locus Body. Cold Spring Harbor Perspectives in Biology *2*, a000653–a000653. 10.1101/cshperspect.a000653.

9. Harris, M.E., Böhni, R., Schneiderman, M.H., Ramamurthy, L., Schümperli, D., and Marzluff, W.F. (1991). Regulation of histone mRNA in the unperturbed cell cycle: evidence suggesting control at two posttranscriptional steps. VOL ., 9.

10. Gurard-Levin, Z.A., Quivy, J.-P., and Almouzni, G. (2014). Histone Chaperones: Assisting Histone Traffic and Nucleosome Dynamics. Annu. Rev. Biochem. *83*, 487–517. 10.1146/annurev-biochem-060713-035536.

11. Hammond, C.M., Strømme, C.B., Huang, H., Patel, D.J., and Groth, A. (2017). Histone chaperone networks shaping chromatin function. Nat Rev Mol Cell Biol *18*, 141–158. 10.1038/nrm.2016.159.

12. Moggs, J.G., Grandi, P., Quivy, J.-P., Jónsson, Z.O., Hübscher, U., Becker, P.B., and Almouzni, G. (2000). A CAF-1–PCNA-Mediated Chromatin Assembly Pathway Triggered by Sensing DNA Damage. Mol Cell Biol *20*, 1206–1218. 10.1128/MCB.20.4.1206-1218.2000.

13. Smith, S., and Stillman, B. (1989). Purification and characterization of CAF-I, a human cell factor required for chromatin assembly during DNA replication in vitro. Cell *58*, 15–25. 10.1016/0092-8674(89)90398-X.

14. Abascal, F., Corpet, A., Gurard-Levin, Z.A., Juan, D., Ochsenbein, F., Rico, D., Valencia, A., and Almouzni, G. (2013). Subfunctionalization via Adaptive Evolution Influenced by Genomic Context: The Case of Histone Chaperones ASF1a and ASF1b. Molecular Biology and Evolution *30*, 1853–1866. 10.1093/molbev/mst086.

15. Le, S., Davis, C., Konopka, J.B., and Sternglanz, R. (1997). Two New S-Phase-Specific Genes fromSaccharomyces cerevisiae. Yeast *13*, 1029–1042. 10.1002/(SICI)1097-0061(19970915)13:11<1029::AID-YEA160>3.0.CO;2-1.

16. Tagami, H., Ray-Gallet, D., Almouzni, G., and Nakatani, Y. (2004). Histone H3.1 and H3.3 Complexes Mediate Nucleosome Assembly Pathways Dependent or Independent of DNA Synthesis. Cell *116*, 51–61. 10.1016/S0092-8674(03)01064-X.

17. Mello, J.A., Silljé, H.H.W., Roche, D.M.J., Kirschner, D.B., Nigg, E.A., and Almouzni, G. (2002). Human Asf1 and CAF- 1 interact and synergize in a repair- coupled nucleosome assembly pathway. EMBO Rep *3*, 329–334. 10.1093/embo-reports/kvf068.

18. Tyler, J.K., Adams, C.R., Chen, S.-R., Kobayashi, R., Kamakaka, R.T., and Kadonaga, J.T. (1999). The RCAF complex mediates chromatin assembly during DNA replication and repair. Nature *402*, 555–560. 10.1038/990147.

19. Ahmad, K., and Henikoff, S. (2002). The Histone Variant H3.3 Marks Active Chromatin by Replication-Independent Nucleosome Assembly. Molecular Cell *9*, 1191–1200. 10.1016/S1097-2765(02)00542-7.

20. Tang, Y., Poustovoitov, M.V., Zhao, K., Garfinkel, M., Canutescu, A., Dunbrack, R., Adams, P.D., and Marmorstein, R. (2006). Structure of a human ASF1a–HIRA complex and insights into specificity of histone chaperone complex assembly. Nat Struct Mol Biol *13*, 921–929. 10.1038/nsmb1147.

21. Clément, C., Orsi, G.A., Gatto, A., Boyarchuk, E., Forest, A., Hajj, B., Miné-Hattab, J., Garnier, M., Gurard-Levin, Z.A., Quivy, J.-P., et al. (2018). High-resolution visualization of H3 variants during replication reveals their controlled recycling. Nat Commun *9*, 3181. 10.1038/s41467-018-05697-1.

22. Groth, A., Corpet, A., Cook, A.J.L., Roche, D., Bartek, J., Lukas, J., and Almouzni, G. (2007). Regulation of Replication Fork Progression Through Histone Supply and Demand. Science *318*, 1928–1931. 10.1126/science.1148992.

23. Torné, J., Ray-Gallet, D., Boyarchuk, E., Garnier, M., Le Baccon, P., Coulon, A., Orsi, G.A., and Almouzni, G. (2020). Two HIRA-dependent pathways mediate H3.3 de novo deposition and recycling during transcription. Nat Struct Mol Biol *27*, 1057–1068. 10.1038/s41594-020-0492-7.

24. Groth, A., Ray-Gallet, D., Quivy, J.-P., Lukas, J., Bartek, J., and Almouzni, G. (2005). Human Asf1 Regulates the Flow of S Phase Histones during Replicational Stress. Molecular Cell *17*, 301–311. 10.1016/j.molcel.2004.12.018.

25. Sutton, A., Bucaria, J., Osley, M.A., and Sternglanz, R. (2001). Yeast ASF1 Protein Is Required for Cell Cycle Regulation of Histone Gene Transcription. Genetics *158*, 587–596. 10.1093/genetics/158.2.587.

26. Barcaroli, D., Bongiorno-Borbone, L., Terrinoni, A., Hofmann, T.G., Rossi, M., Knight, R.A., Matera, A.G., Melino, G., and De Laurenzi, V. (2006). FLASH is required for histone transcription and S-phase progression. Proc. Natl. Acad. Sci. U.S.A. *103*, 14808–14812. 10.1073/pnas.0604227103.

27. Yang, X., Burch, B.D., Yan, Y., Marzluff, W.F., and Dominski, Z. (2009). FLASH, a Proapoptotic Protein Involved in Activation of Caspase-8, Is Essential for 3′ End Processing of Histone Pre-mRNAs. Molecular Cell *36*, 267–278. 10.1016/j.molcel.2009.08.016.

28. Koç, A., Wheeler, L.J., Mathews, C.K., and Merrill, G.F. (2004). Hydroxyurea Arrests DNA Replication by a Mechanism That Preserves Basal dNTP Pools. Journal of Biological Chemistry *279*, 223–230. 10.1074/jbc.M303952200.

29. Gao, Y., Gan, H., Lou, Z., and Zhang, Z. (2018). Asf1a resolves bivalent chromatin domains for the induction of lineage-specific genes during mouse embryonic stem cell differentiation. Proc. Natl. Acad. Sci. U.S.A. *115*. 10.1073/pnas.1801909115.

30. Armstrong, C., Passanisi, V.J., Ashraf, H.M., and Spencer, S.L. (2023). Cyclin E/CDK2 and feedback from soluble histone protein regulate the S phase burst of histone biosynthesis. Cell Reports *42*, 112768. 10.1016/j.celrep.2023.112768.

31. Sullivan, K.D., Mullen, T.E., Marzluff, W.F., and Wagner, E.J. (2009). Knockdown of SLBP results in nuclear retention of histone mRNA. RNA *15*, 459–472. 10.1261/rna.1205409.

32. Sànchez, R., and Marzluff, W.F. (2002). The Stem-Loop Binding Protein Is Required for Efficient Translation of Histone mRNA In Vivo and In Vitro. Molecular and Cellular Biology *22*, 7093–7104. 10.1128/MCB.22.20.7093-7104.2002.

33. Nelson, D.M., Ye, X., Hall, C., Santos, H., Ma, T., Kao, G.D., Yen, T.J., Harper, J.W., and Adams, P.D. (2002). Coupling of DNA Synthesis and Histone Synthesis in S Phase Independent of Cyclin/cdk2 Activity. Mol Cell Biol *22*, 7459–7472. 10.1128/MCB.22.21.7459-7472.2002.

34. Morales Torres, C., Wu, M.Y., Hobor, S., Wainwright, E.N., Martin, M.J., Patel, H., Grey, W., Grönroos, E., Howell, S., Carvalho, J., et al. (2020). Selective inhibition of cancer cell self-renewal through a Quisinostat-histone H1.0 axis. Nat Commun *11*, 1792. 10.1038/s41467-020-15615-z.

35. Torres, C.M., Biran, A., Burney, M.J., Patel, H., Henser-Brownhill, T., Cohen, A.-H.S., Li, Y., Ben-Hamo, R., Nye, E., Spencer-Dene, B., et al. (2016). The linker histone H1.0 generates epigenetic and functional intratumor heterogeneity. Science *353*, aaf1644. 10.1126/science.aaf1644.

36. Ma, T., Van Tine, B.A., Wei, Y., Garrett, M.D., Nelson, D., Adams, P.D., Wang, J., Qin, J., Chow, L.T., and Harper, J.W. (2000). Cell cycle–regulated phosphorylation of p220 ^{NPAT} by cyclin E/Cdk2 in Cajal bodies promotes histone gene transcription. Genes Dev. *14*, 2298–2313. 10.1101/gad.829500.

37. Zhao, J., Kennedy, B.K., Lawrence, B.D., Barbie, D.A., Matera, A.G., Fletcher, J.A., and Harlow, E. (2000). NPAT links cyclin E–Cdk2 to the regulation of replication-dependent histone gene transcription. Genes Dev. *14*, 2283–2297. 10.1101/gad.827700.

38. Narita, T., Yung, T.M.C., Yamamoto, J., Tsuboi, Y., Tanabe, H., Tanaka, K., Yamaguchi, Y., and Handa, H. (2007). NELF Interacts with CBC and Participates in 3′ End Processing of Replication-Dependent Histone mRNAs. Molecular Cell *26*, 349–365. 10.1016/j.molcel.2007.04.011.

39. Romeo, V., Griesbach, E., and Schümperli, D. (2014). CstF64: Cell Cycle Regulation and Functional Role in 3′ End Processing of Replication-Dependent Histone mRNAs. Mol Cell Biol *34*, 4272–4284. 10.1128/MCB.00791-14.

40. Saldi, T., Fong, N., and Bentley, D.L. (2018). Transcription elongation rate affects nascent histone pre-mRNA folding and 3′ end processing. Genes Dev. *32*, 297–308. 10.1101/gad.310896.117.

41. Sullivan, E., Santiago, C., Parker, E.D., Dominski, Z., Yang, X., Lanzotti, D.J., Ingledue, T.C., Marzluff, W.F., and Duronio, R.J. (2001). *Drosophila* stem loop binding protein coordinates accumulation of mature histone mRNA with cell cycle progression. Genes Dev. *15*, 173–187. 10.1101/gad.862801.

42. Ogami, K., Chen, Y., and Manley, J. (2018). RNA Surveillance by the Nuclear RNA Exosome: Mechanisms and Significance. ncRNA *4*, 8. 10.3390/ncrna4010008.

43. Ogami, K., and Suzuki, H.I. (2021). Nuclear RNA Exosome and Pervasive Transcription: Dual Sculptors of Genome Function. IJMS *22*, 13401. 10.3390/ijms222413401.

44. Wagner, E.J., Burch, B.D., Godfrey, A.C., Salzler, H.R., Duronio, R.J., and Marzluff, W.F. (2007). A Genome-wide RNA Interference Screen Reveals that Variant Histones Are Necessary for Replication-Dependent Histone Pre-mRNA Processing. Molecular Cell *28*, 692–699. 10.1016/j.molcel.2007.10.009.

45. Mejlvang, J., Feng, Y., Alabert, C., Neelsen, K.J., Jasencakova, Z., Zhao, X., Lees, M., Sandelin, A., Pasero, P., Lopes, M., et al. (2014). New histone supply regulates replication fork speed and PCNA unloading. Journal of Cell Biology *204*, 29–43. 10.1083/jcb.201305017.

46. Hoek, M., and Stillman, B. (2003). Chromatin assembly factor 1 is essential and couples chromatin assembly to DNA replication *in vivo*. Proc. Natl. Acad. Sci. U.S.A. *100*, 12183–12188. 10.1073/pnas.1635158100.

47. Sherwood, P.W. (1993). Characterization of HIRJ and HIR2, Two Genes Required for Regulation of Histone Gene Transcription in Saccharomyces cerevisiae. MOL. CELL. BIOL. *13*, 11.

48. Spector, M.S., Raff, A., DeSilva, H., Lee, K., and Osley, M.A. (1997). Hir1p and Hir2p function as transcriptional corepressors to regulate histone gene transcription in the Saccharomyces cerevisiae cell cycle. Mol Cell Biol *17*, 545–552. 10.1128/MCB.17.2.545.

49. Cook, A.J.L., Gurard-Levin, Z.A., Vassias, I., and Almouzni, G. (2011). A Specific Function for the Histone Chaperone NASP to Fine-Tune a Reservoir of Soluble H3-H4 in the Histone Supply Chain. Molecular Cell *44*, 918–927. 10.1016/j.molcel.2011.11.021.

50. Ray-Gallet, D., and Almouzni, G. (2022). H3–H4 histone chaperones and cancer. Current Opinion in Genetics & Development *73*, 101900. 10.1016/j.gde.2022.101900.

51. Fuchs, G., Voichek, Y., Rabani, M., Benjamin, S., Gilad, S., Amit, I., and Oren, M. (2015). Simultaneous measurement of genome-wide transcription elongation speeds and rates of RNA polymerase II transition into active elongation with 4sUDRB-seq. Nat Protoc *10*, 605–618. 10.1038/nprot.2015.035.

52. Polo, S.E., Roche, D., and Almouzni, G. (2006). New Histone Incorporation Marks Sites of UV Repair in Human Cells. Cell *127*, 481–493. 10.1016/j.cell.2006.08.049.

53. Ray-Gallet, D., Woolfe, A., Vassias, I., Pellentz, C., Lacoste, N., Puri, A., Schultz, D.C., Pchelintsev, N.A., Adams, P.D., Jansen, L.E.T., et al. (2011). Dynamics of Histone H3 Deposition In Vivo Reveal

a Nucleosome Gap-Filling Mechanism for H3.3 to Maintain Chromatin Integrity. Molecular Cell *44*, 928–941. 10.1016/j.molcel.2011.12.006.

54. Ruepp, M.-D., Vivarelli, S., Pillai, R.S., Kleinschmidt, N., Azzouz, T.N., Barabino, S.M.L., and Schümperli, D. (2010). The 68 kDa subunit of mammalian cleavage factor I interacts with the U7 small nuclear ribonucleoprotein and participates in 3′-end processing of animal histone mRNAs. Nucleic Acids Research *38*, 7637–7650. 10.1093/nar/gkq613.

55. Simeonova, I., Lejour, V., Bardot, B., Bouarich-Bourimi, R., Morin, A., Fang, M., Charbonnier, L., and Toledo, F. (2012). Fuzzy Tandem Repeats Containing p53 Response Elements May Define Species-Specific p53 Target Genes. PLoS Genet *8*, e1002731. 10.1371/journal.pgen.1002731.

56. Love, M.I., Huber, W., and Anders, S. (2014). Moderated estimation of fold change and dispersion for RNA-seq data with DESeq2. Genome Biol *15*, 550. 10.1186/s13059-014-0550-8.

57. Martini, E., Roche, D.M.J., Marheineke, K., Verreault, A., and Almouzni, G. (1998). Recruitment of Phosphorylated Chromatin Assembly Factor 1 to Chromatin after UV Irradiation of Human Cells. Journal of Cell Biology *143*, 563–575. 10.1083/jcb.143.3.563.

FIGURE 1

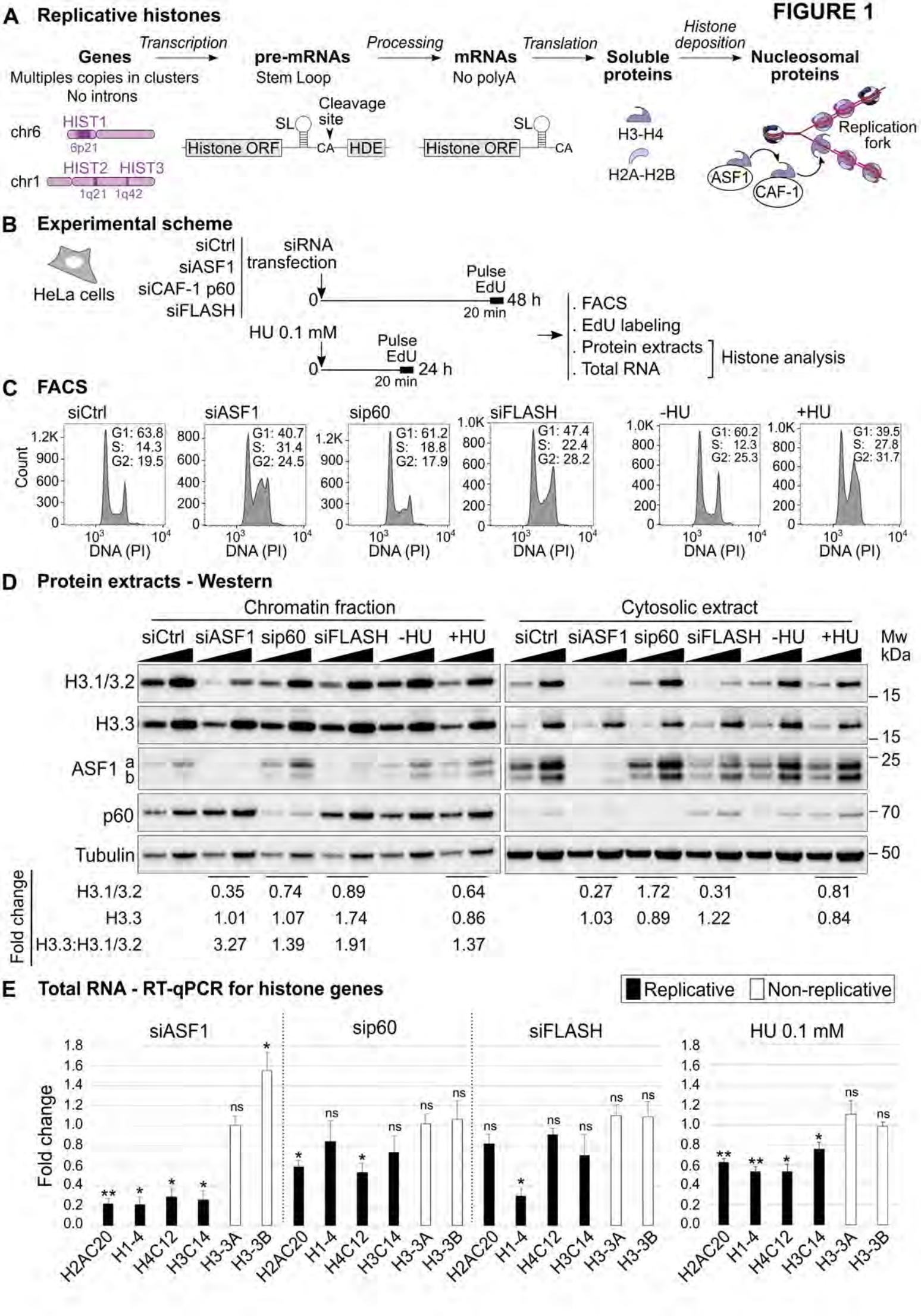
A Replicative histones
Genes
Multiples copies in clusters
No introns
Transcription
pre-mRNAs
Stem Loop
Processing
mRNAs
No polyA
Translation
Soluble proteins
Histone deposition
Nucleosomal proteins
chr6
HIST1
6p21
chr1
HIST2 HIST3
1q21 1q42
Cleavage site
SL
Histone ORF
CA
HDE
H3-H4
H2A-H2B
Replication fork
ASF1
CAF-1
B Experimental scheme
HeLa cells
siCtrl
siASF1
siCAF-1 p60
siFLASH
siRNA transfection
Pulse EdU
20 min
48 h
HU 0.1 mM
24 h
. FACS
. EdU labeling
. Protein extracts
. Total RNA
Histone analysis
C FACS
siCtrl
siASF1
sip60
siFLASH
-HU
+HU
Count
G1: 63.8
S: 14.3
G2: 19.5
G1: 40.7
S: 31.4
G2: 24.5
G1: 61.2
S: 18.8
G2: 17.9
G1: 47.4
S: 22.4
G2: 28.2
G1: 60.2
S: 12.3
G2: 25.3
G1: 39.5
S: 27.8
G2: 31.7
DNA (PI)
D Protein extracts - Western
Chromatin fraction
Cytosolic extract
Mw kDa
H3.1/3.2
H3.3
ASF1 a
b
p60
Tubulin
15
15
25
70
50
Fold change
H3.1/3.2 0.35 0.74 0.89 0.64 0.27 1.72 0.31 0.81
H3.3 1.01 1.07 1.74 0.86 1.03 0.89 1.22 0.84
H3.3:H3.1/3.2 3.27 1.39 1.91 1.37
E Total RNA - RT-qPCR for histone genes
Replicative
Non-replicative
siASF1
sip60
siFLASH
HU 0.1 mM
Fold change
ns
H2AC20
H1-4
H4C12
H3C14
H3-3A
H3-3B

FIGURE 2

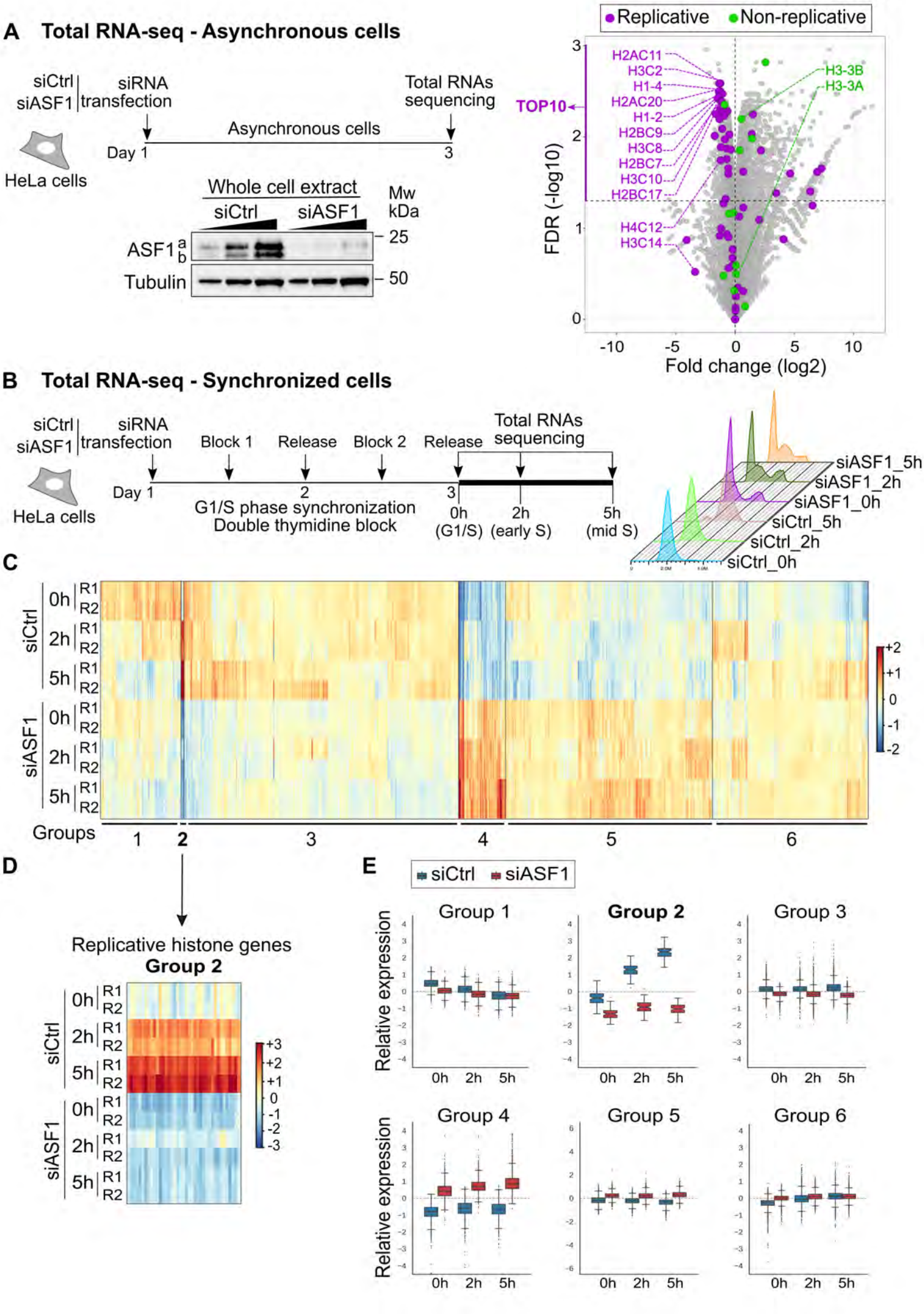
A Total RNA-seq - Asynchronous cells
siCtrl
siASF1
siRNA transfection
Total RNAs sequencing
Asynchronous cells
Day 1
3
HeLa cells
Whole cell extract
siCtrl
siASF1
Mw kDa
ASF1 a
b
Tubulin
25
50
Replicative
Non-replicative
TOP10
H2AC11
H3C2
H1-4
H2AC20
H1-2
H2BC9
H3C8
H2BC7
H3C10
H2BC17
H4C12
H3C14
H3-3B
H3-3A
FDR (-log10)
Fold change (log2)
B Total RNA-seq - Synchronized cells
siCtrl
siASF1
siRNA transfection
Block 1
Release
Block 2
Release
Total RNAs sequencing
Day 1
2
3
G1/S phase synchronization
Double thymidine block
0h (G1/S)
2h (early S)
5h (mid S)
HeLa cells
siASF1_5h
siASF1_2h
siASF1_0h
siCtrl_5h
siCtrl_2h
siCtrl_0h
C
siCtrl
siASF1
0h
2h
5h
R1
R2
Groups
1
2
3
4
5
6
+2
+1
0
-1
-2
D
Replicative histone genes
Group 2
+3
+2
+1
0
-1
-2
-3
E
siCtrl
siASF1
Group 1
Group 2
Group 3
Group 4
Group 5
Group 6
Relative expression
0h
2h
5h

FIGURE 3

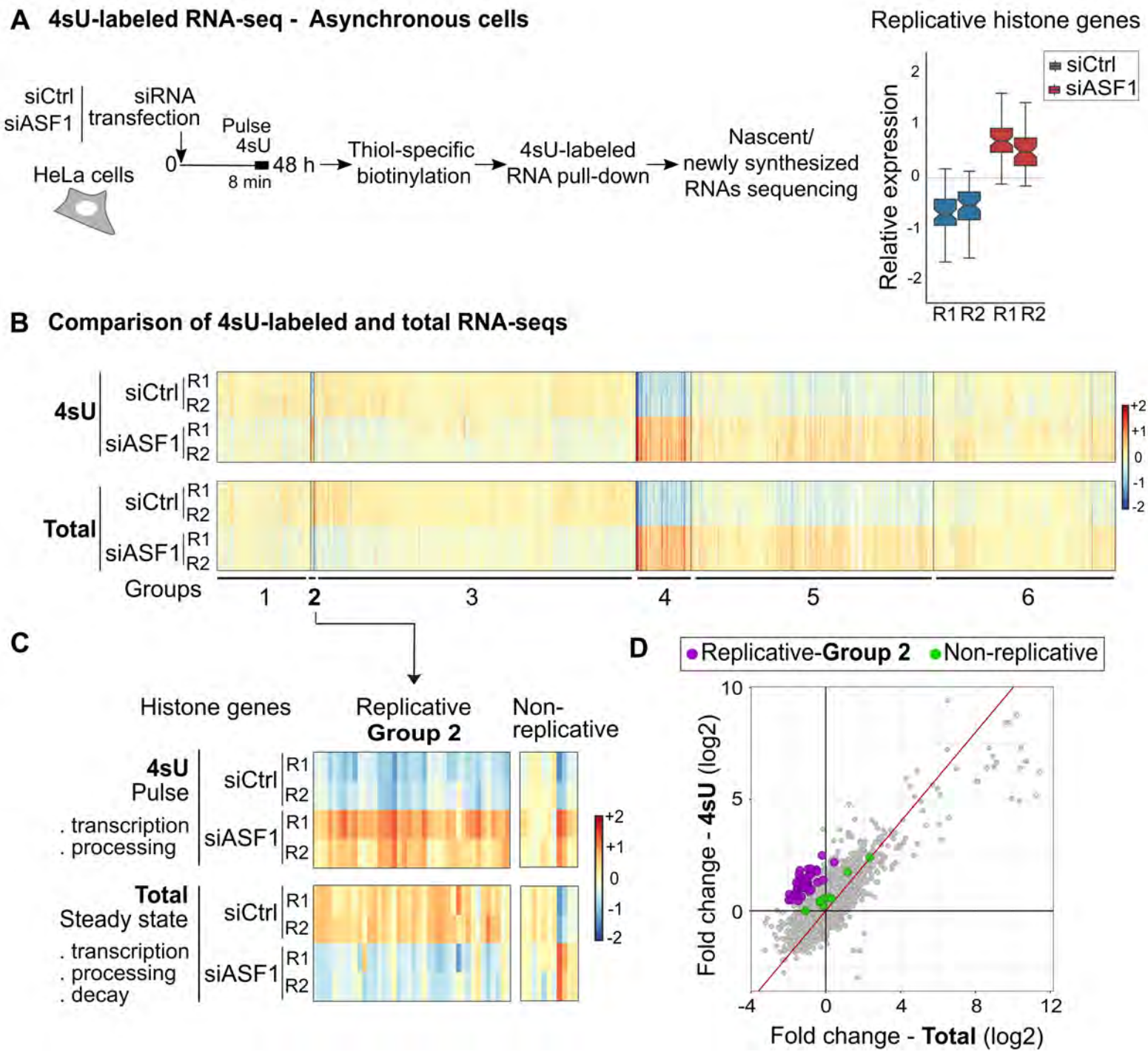
A 4sU-labeled RNA-seq - Asynchronous cells
siCtrl
siASF1
siRNA transfection
HeLa cells
0
Pulse 4sU
8 min
48 h
Thiol-specific biotinylation
4sU-labeled RNA pull-down
Nascent/ newly synthesized RNAs sequencing
Replicative histone genes
siCtrl
siASF1
Relative expression
R1 R2 R1 R2
B Comparison of 4sU-labeled and total RNA-seqs
4sU
Total
siCtrl
siASF1
R1
R2
Groups
1
2
3
4
5
6
C
Histone genes
Replicative Group 2
Non-replicative
4sU Pulse
. transcription
. processing
Total Steady state
. transcription
. processing
. decay
D
Replicative-Group 2
Non-replicative
Fold change - 4sU (log2)
Fold change - Total (log2)

FIGURE 4

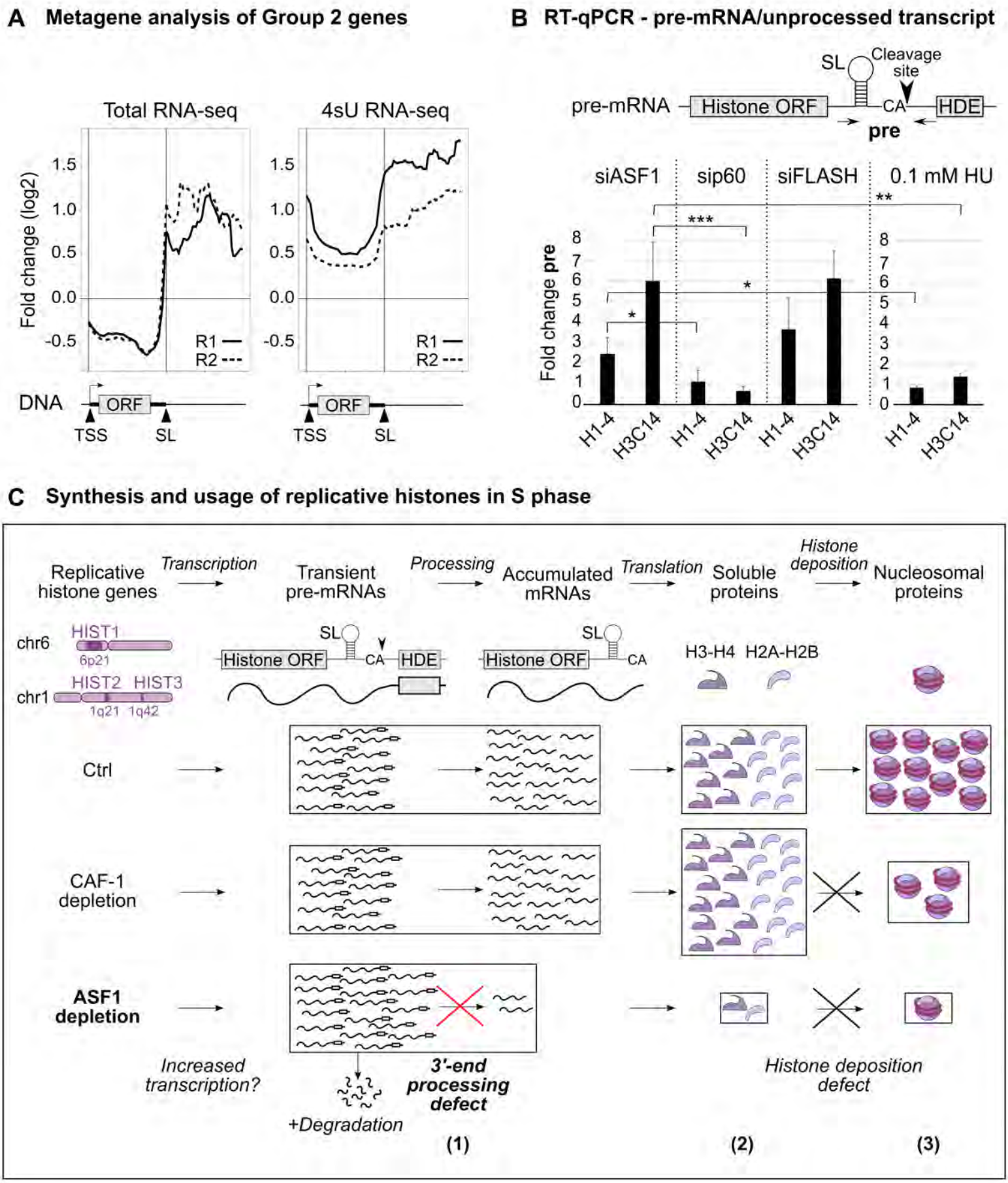
A Metagene analysis of Group 2 genes
Total RNA-seq
4sU RNA-seq
Fold change (log2)
1.5
1.0
0.5
0.0
-0.5
R1
R2
DNA
ORF
TSS
SL
B RT-qPCR - pre-mRNA/unprocessed transcript
SL
Cleavage site
pre-mRNA
Histone ORF
CA
HDE
pre
siASF1
sip60
siFLASH
0.1 mM HU
Fold change pre
H1-4
H3C14
C Synthesis and usage of replicative histones in S phase
Replicative histone genes
Transcription
Transient pre-mRNAs
Processing
Accumulated mRNAs
Translation
Soluble proteins
Histone deposition
Nucleosomal proteins
chr6
HIST1
6p21
chr1
HIST2 HIST3
1q21 1q42
Histone ORF
CA
HDE
H3-H4 H2A-H2B
Ctrl
CAF-1 depletion
ASF1 depletion
Increased transcription?
3'-end processing defect
+Degradation
Histone deposition defect
(1)
(2)
(3)

SUPPLEMENTAL INFORMATION

Regulation of replicative histone RNA metabolism by the histone chaperone ASF1

Shweta Mendiratta, Dominique Ray-Gallet, Sébastien Lemaire, Alberto Gatto, Audrey Forest, Maciej A. Kerlin and Geneviève Almouzni

SUPPLEMENTAL FIGURES

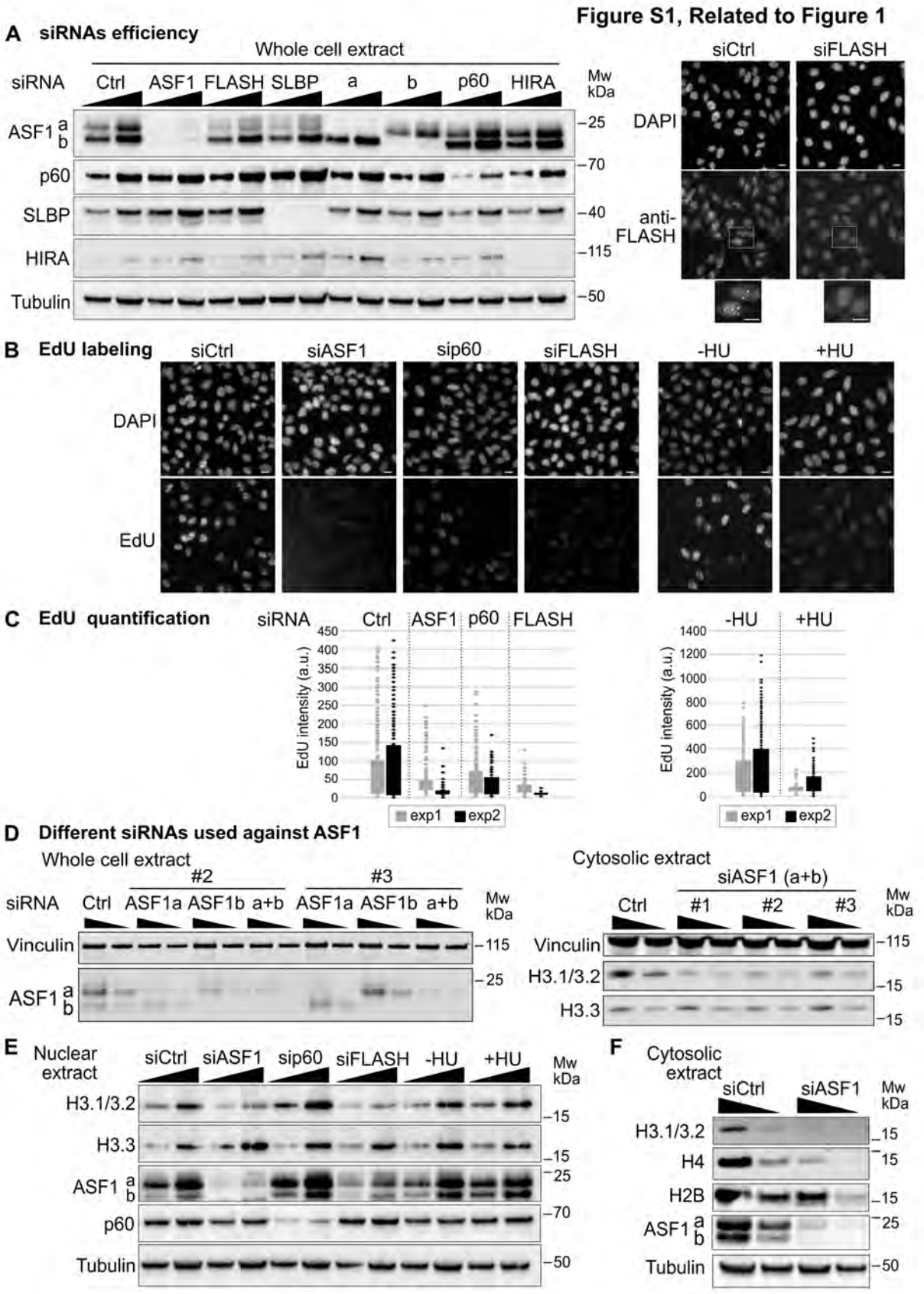

Figure S1. ASF1 depletion reduces replicative histones at the levels of both soluble protein and total RNA, Related to Figure 1

(A) (Left) Western blot analysis of whole HeLa cell extract from siCtrl-, siASF1-, siFLASH-, siSLBP-, siASF1a-, siASF1b-, sip60 (CAF-1)- or siHIRA-treated cells showing the efficiency of depletions. We used extracts corresponding to the same number of cells (1x and 2x) and γ-tubulin as loading control. Following both FLASH and SLBP depletions, ASF1a and ASF1b signals decreased while slower migrating bands, likely phosphorylated forms [S1,S2], appeared in line with S phase cell accumulation. However, HU-treated cells, also accumulate in S phase, and do not show this, thus we consider that other effects deserve investigation. **(Right)** Immunofluorescence analysis of FLASH in siCtrl- or siFLASH-treated HeLa cells. The nuclei are visualized by DAPI staining. The insets represent enlarged images of selected cells. Scale bar 10 μm. **(B)** EdU labeling of replicating cells in Ctrl-, ASF1-, sip60- or FLASH-depleted cells and in control (-HU) and HU-treated (+HU) cells. Scale bar 10 μm. **(C)** Quantification of EdU fluorescence intensity in arbitrary units (a.u.) from two siRNA- and two HU-treatment experiments (exp1 and exp2). **(D) (Left)** Western blot analysis of whole cell extracts from HeLa cells harvested 48 hrs after siRNA transfection (siCtrl, siASF1a (#2 or #3), siASF1b (#2 or #3) or ASF1a+b (#2 or #3)). We used extracts corresponding to the same number of cells (1x and 2x). We examined ASF1a and ASF1b and used vinculin as loading control. **(Right)** Western blot analysis of cytosolic extract from HeLa cells harvested 48 hrs after siRNA transfection with siCtrl or ASF1a+b (#1, #2 or #3). We examined the replicative histones H3.1/H3.2 and the non-replicative histone H3.3. We used 10 and 20 μg of extracts and vinculin as loading control. **(E)** Western blot analysis of nuclear extract from HeLa cells harvested 48 hrs after siRNA transfection (siCtrl, siASF1, siCAF-1-p60 or siFLASH) or 24 hrs after HU treatment (+HU) or control (-HU). We examined ASF1a and b, p60, the replicative histones H3.1/H3.2 and the non-replicative histone H3.3. We used 10 and 20 μg of extracts and γ-tubulin as loading control. **(F)** Western blot analysis of cytosolic extract from HeLa cells harvested 48 hrs after siRNA transfection (siCtrl or siASF1). We examined the replicative histones H3.1/H3.2, H4 and H2B. We used 10 and 20 μg of extracts and γ-tubulin as loading control.

Figure S2, Related to Figure 1

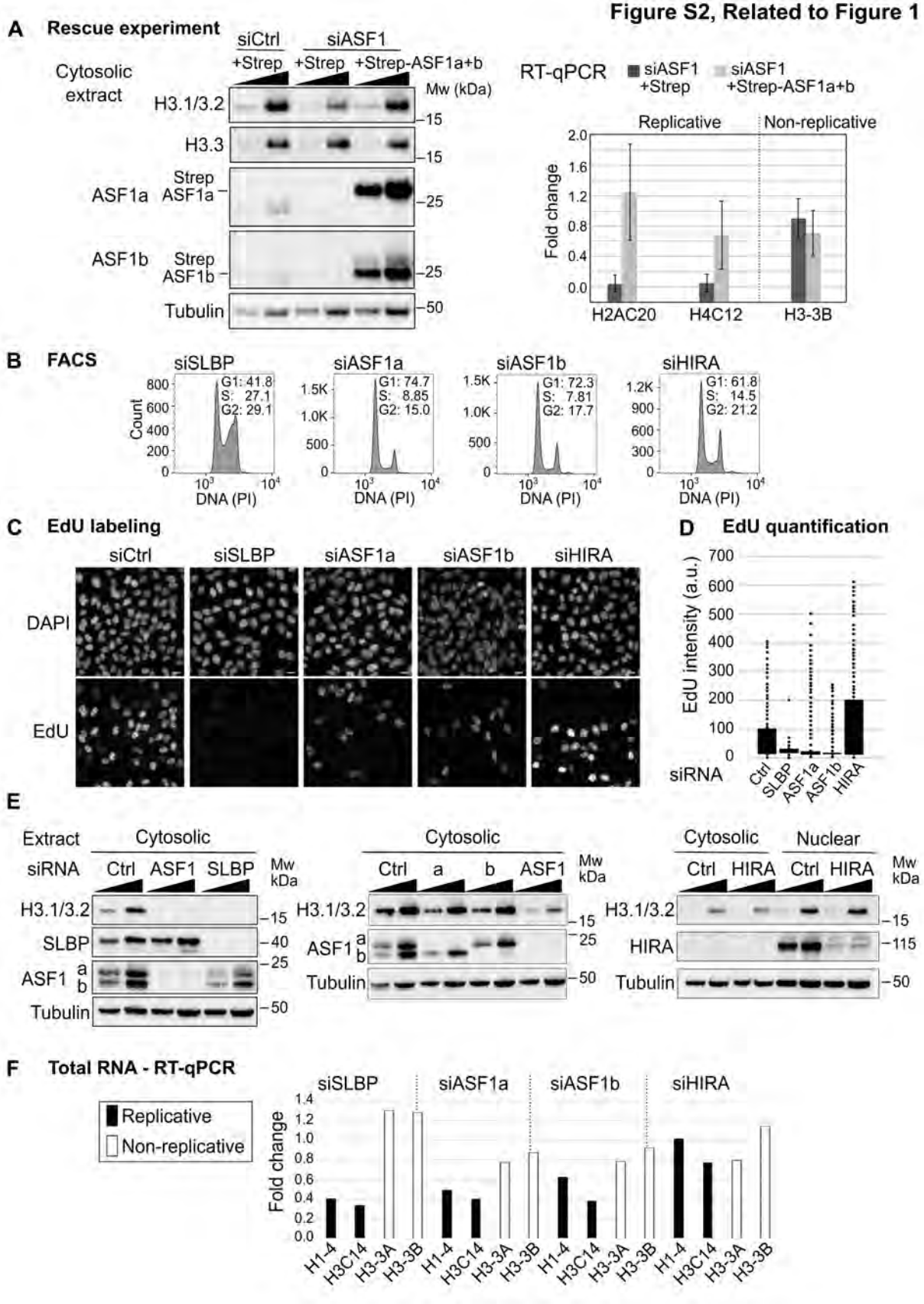

Figure S2. ASF1 depletion rescue and impact of siSLBP, siASF1a, siASF1b and siHIRA transfections on replicative histones, Related to Figure 1

(A) Rescue experiment. HeLa cells were transfected with siRNAs (siCtrl or siASF1), then, 24 hrs later with expression vectors, either with the empty vector pEXPR-IBA105 (Strep) or with those expressing Onestrep-ASF1a and Onestrep-ASF1b (Strep-ASF1a+b). The cells were harvested 48 hrs after siRNA transfection and either proteins or total RNA were prepared. **(Left)** Western blot analysis of cytosolic extract. Two amounts 1x and 2x were loaded. We examined ASF1a and ASF1b, replicative histones H3.1/H3.2 and H4 and the non-replicative H3.3 and used γ-tubulin as loading control. **(Right)** RT-qPCR analysis. Individual histone genes are the replicative H2AC20 (H2A type 2-C) and H4C12 (H4) and the non-replicative H3-3B (H3.3). The fold change in transcript levels as compared to siCtrl+Strep corresponds to the mean of two independent biological replicate experiments. **(B)** FACS analysis of the cells 48 hrs after siRNAs transfection (siSLBP, siASF1a, siASF1b or siHIRA). We stained cells with PI and analyzed DNA content by flow cytometry. Percentages of cells in G1, S and G2/M are indicated. **(C)** EdU labeling of replicating cells as described in panel (B) for SLBP-, ASF1a-, ASF1-b and HIRA-depleted cells. Scale bar 10 μm. **(D)** EdU fluorescence quantification as described in panel (C) for SLBP-, ASF1a-, ASF1-b and HIRA-depleted cells. **(E)** Western blots of cytosolic and nuclear extracts from HeLa cells harvested 48 hrs after siRNA transfection (siCtrl, siASF1, siASF1a, siASF1b, siSLBP or siHIRA). We used 10 and 20 μg of extracts and γ-tubulin as loading control. **(F)** RT-qPCR analysis of histone RNA levels. Total RNA was isolated from HeLa cells harvested 48 hrs after siRNA transfection (siCtrl, siSLBP, siASF1a, siASF1b or siHIRA). We show individual histone genes: the replicative genes (in black) H2AC20 and H3C14 and the non-replicative genes (in white) H3-3A and H3-3B. Fold changes in transcript levels for siSLBP, siASF1a, siASF1b and siHIRA transfected cells relative to siCtrl are shown.

Figure S3, Related to Figure 2

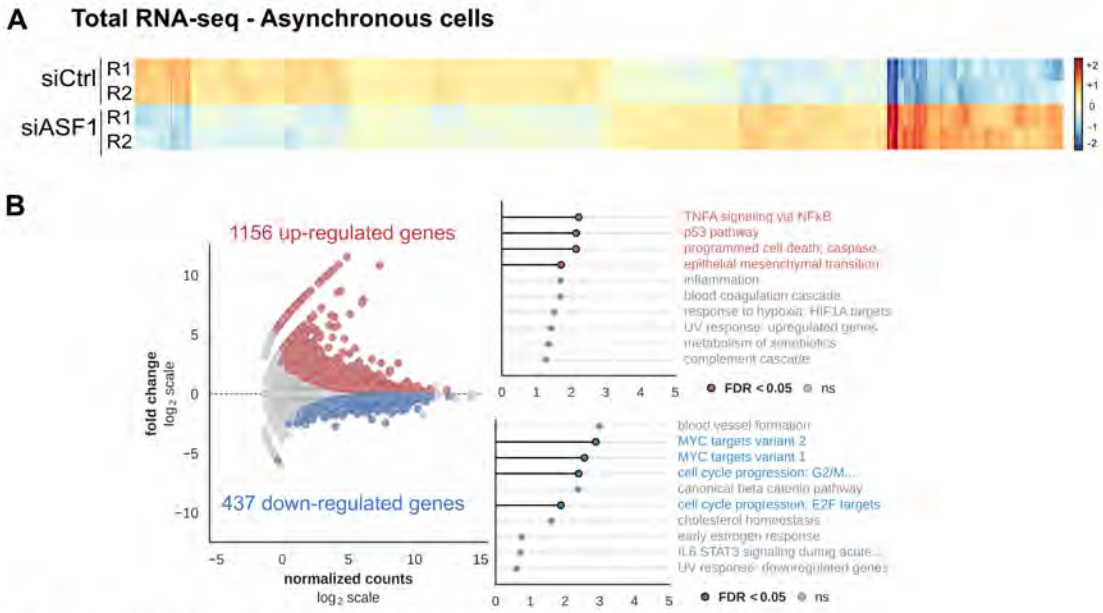

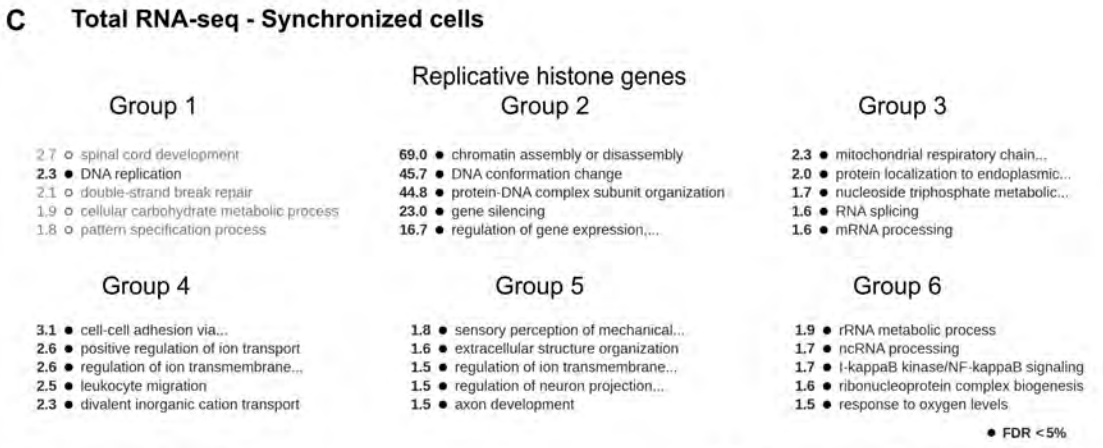

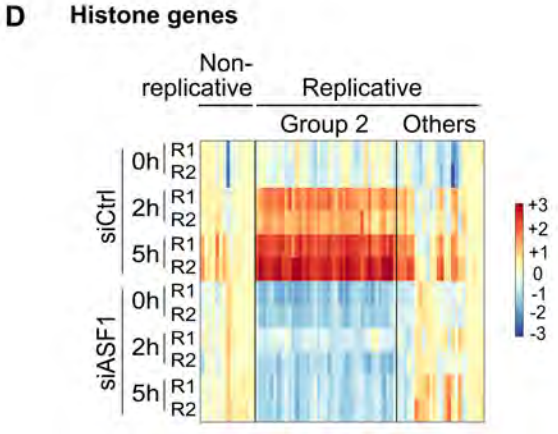

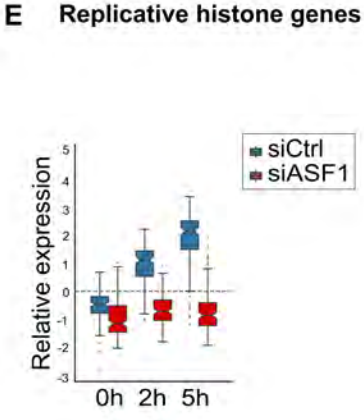

Figure S3. Impact of ASF1 depletion on transcriptome - RNA-seq data from asynchronous and synchronized HeLa cells in siCtrl and siASF1 conditions, Related to Figure 2

(A) Heat map showing hierarchical clustering of samples (rows) and differentially expressed genes (columns) between siCtrl and siASF1 conditions in asynchronous cells, including all genes showing significant differences at FDR < 0.05. The color gradient is proportional to the expression of each gene in each sample, relative to their average across all samples (log2 normalized counts, mean-centered): from blue (lower than average) to red (higher than average). The experiment was performed in duplicate, replicate 1 (R1) and replicate 2 (R2). **(B) (Left)** MA plot showing log2 fold change between siASF1 and siCtrl versus baseline expression levels across all genes. Differentially expressed genes at FDR < 0.05 are highlighted in blue (downregulated) or red (upregulated). **(Right)** Hallmark signatures associated with the top 100 upregulated (top panel) or downregulated genes (bottom panel), as identified by over-representation analysis (ORA) with WebGestaltR v0.4.2. Signatures showing significant enrichment at FDR < 0.05 are highlighted in red (for upregulated genes) and blue (for downregulated genes). **(C)** Six groups of genes identified by hierarchical clustering from differential gene expression between siASF1 and siCtrl in synchronized HeLa cells (see Figures 2C and 2E). For all groups of genes, the top 5 Gene Ontology (GO) annotations are shown (over-representation analysis with WebGestaltR, v0.4.2). GO terms showing significant enrichment at FDR < 0.05 are highlighted in black. Group 2 corresponds only to replicative histone genes. **(D)** Heat map showing hierarchical clustering of all replicative histone genes and non-replicative histone genes in siCtrl and siASF1 conditions. Color gradient shows expression relative to average as in Figure 2C (log2 normalized counts, mean-centred): from blue (lower than average) to red (higher than average). **(E)** The box plots show the distribution of relative expression levels of all replicative histone genes in siCtrl (in blue) and siASF1 (in red) conditions at 0 (G1/S), 2 and 5 hrs (S phase) after release from the G1/S block (log2 normalized counts, mean-centered across all samples and averaged by experimental condition). See also supplementary Table.

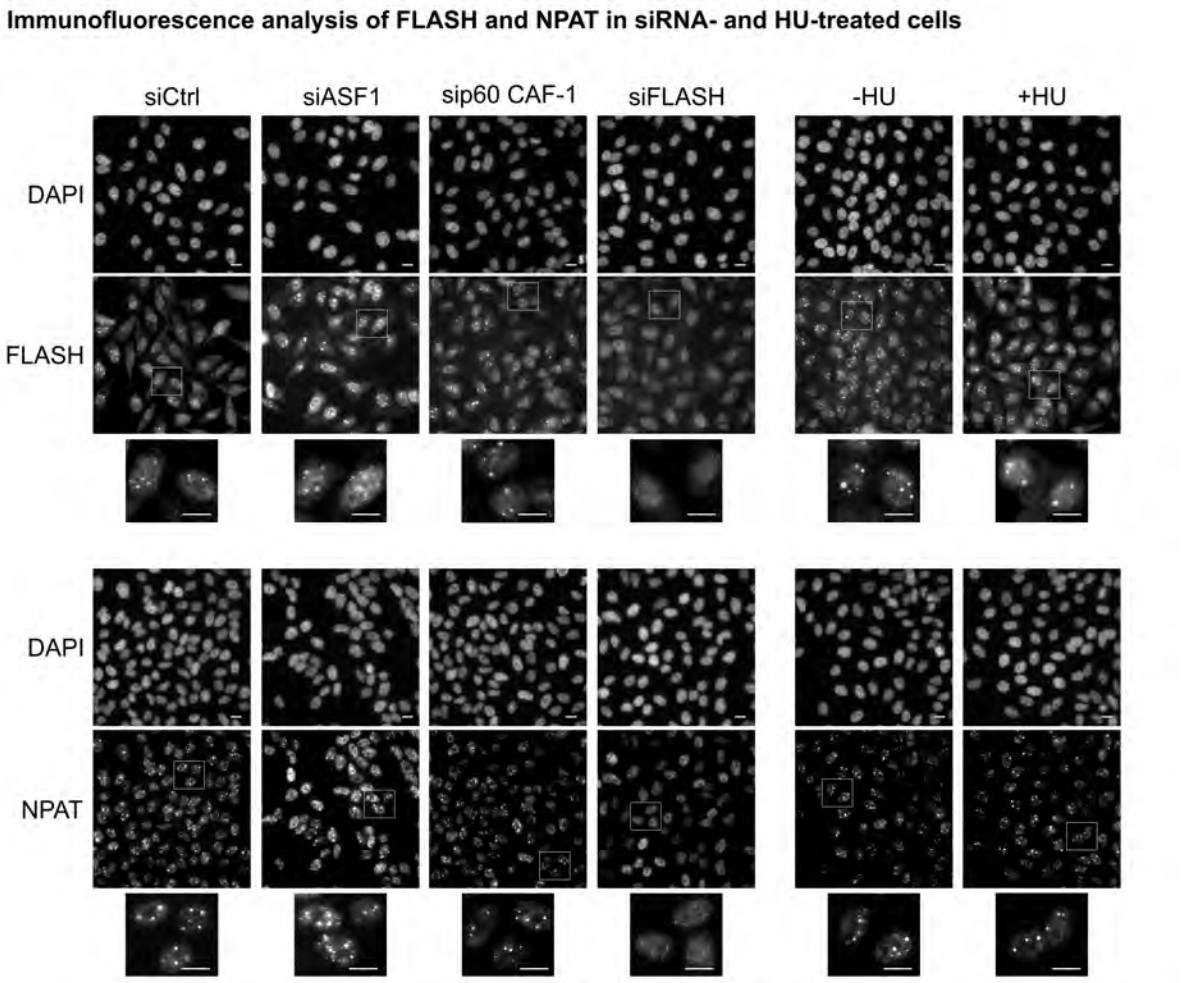

Figure S4. Immunofluorescence analysis of FLASH and NPAT after siRNA and HU treatments, Related to Figure 3

Immunofluorescence analysis of FLASH (top) and NPAT (bottom) in HeLa cells treated with siRNA (siCtrl, siASF1, sip60 CAF1 and siFLASH) or with HU (+HU) and control without drug (-HU). The nuclei are visualized by DAPI staining. The insets represent enlarged images of selected cells. Scale bar 10 μm.

Figure S5, Related to Figure 4

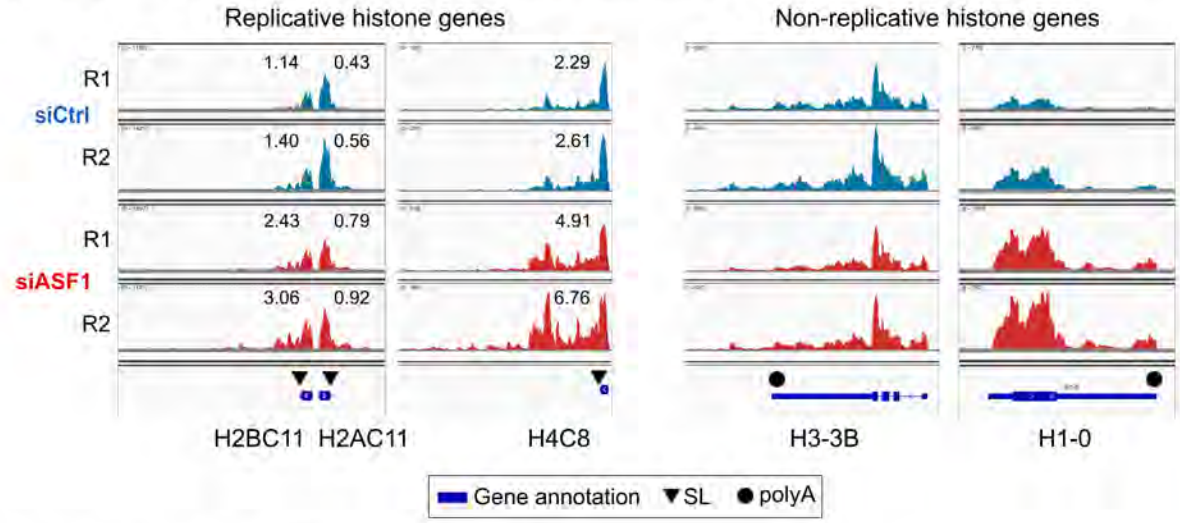

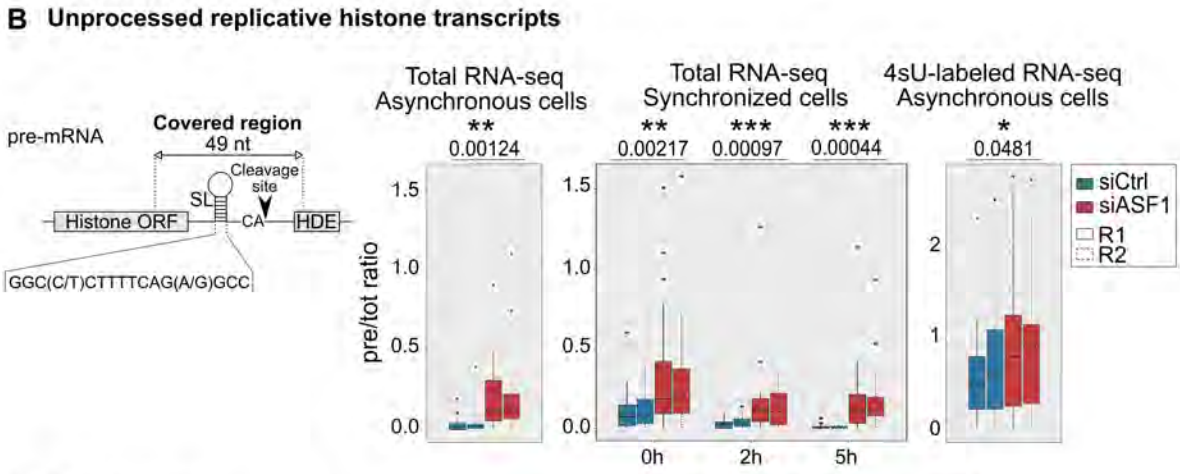

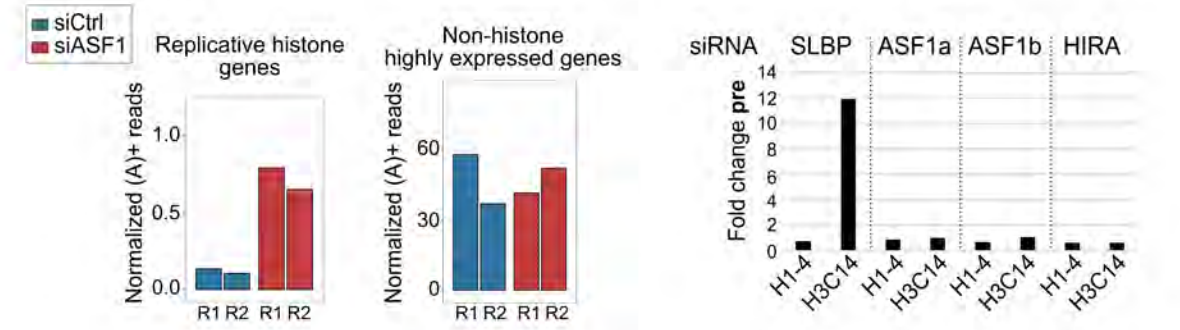

Figure S5. ASF1 depletion affects the 3'-end processing of replicative histone transcripts, Related to Figure 4

(A) Snapshots of 4sU-labeled RNA-seq signal tracks in siCtrl and siASF1 conditions focusing on annotations (blue bars) and regions downstream of the SL of the replicative histone genes H2BC11, H2AC11, H4C8 and the non-replicative histone genes H3-3B and H1-0. Stem loops and polyadenylation sites are respectively indicated by triangles and circles. Numbers above the tracks indicate ratios of the read counts mapping on the region downstream of SL over the read counts mapping the ORF for each replicative histone gene. **(B) (Left)** Scheme showing replicative histone pre-mRNA. The cleavage of the pre-mRNA occurs downstream of the Stem-Loop (SL) and upstream of the Histone Downstream Element (HDE). The detection of the indicated 49 nucleotides in RNA-seq fragments is diagnostic of pre-mRNA/unprocessed replicative histone transcripts. This fragment encompasses the cleavage site, from 20 nucleotides upstream of the SL (16 nt long) to 13 nucleotides downstream of the SL, reaching the HDE. **(Right)** We compared the fractions of unprocessed transcripts between siASF1 and siCtrl conditions using data from our total (~5.7-fold increase) and 4sU-labeled RNA-seqs (~1.34-fold increase) of asynchronous cells and from our total RNA-seq of synchronized cells (~2.8-, ~5- and ~21-fold increases at times 0, 2 and 5 hrs after release). The box plots show the ratio of the number of unprocessed transcripts to total transcripts (total number of reads mapping in each annotated replicative histone gene of Group 2). The results for the two replicates R1 and R2 are shown. The p-values for greater values in siASF1 compared to siCtrl are indicated. **(C)** Levels of oligo/poly(A)+ transcripts for replicative histone genes that are downregulated after ASF1 depletion (left panel) and for highly expressed genes (second decile of most highly expressed genes in synchronized cells) (right panel). We provide the spike-in normalized number of oligo/poly(A)+ reads. The two replicates (R1 and R2) for siCtrl and siASF1 conditions are shown. **(D)** Analysis of replicative histone pre-mRNAs/unprocessed transcripts by RT-qPCR amplifying sequence defined by "pre" primers (Figure 4B) on genes H1-4 and H3C14. We used total RNA isolated from HeLa cells harvested 48 hrs after siRNA transfection (siCtrl, siSLBP, siASF1a, siASF1b or siHIRA). We provided the fold changes in unprocessed transcript levels for siSLBP, siASF1a, siASF1b and siHIRA transfected cells relatively to siCtrl. See also supplementary Table.

SUPPLEMENTAL REFERENCES

S1. Klimovskaia, I.M., Young, C., Strømme, C.B., Menard, P., Jasencakova, Z., Mejlvang, J., Ask, K., Ploug, M., Nielsen, M.L., Jensen, O.N., et al. (2014). Tousled-like kinases phosphorylate Asf1 to promote histone supply during DNA replication. Nat Commun *5*, 3394. 10.1038/ncomms4394.

S2. Silljé, H.H.W., and Nigg, E.A. (2001). Identification of human Asf1 chromatin assembly factors as substrates of Tousled-like kinases. Current Biology *11*, 1068–1073. 10.1016/S0960-9822(01)00298-6.